New Journal of Physics
The open access journal at the forefront of physics

Deutsche Physikalische Gesellschaft DPG
IOP Institute of Physics

Published in partnership with: Deutsche Physikalische Gesellschaft and the Institute of Physics

OPEN ACCESS

RECEIVED
4 August 2015

REVISED
23 November 2015

ACCEPTED FOR PUBLICATION
24 November 2015

PUBLISHED
18 January 2016

PAPER

Neutrino oscillations with the MINOS, MINOS+, T2K, and NOvA experiments

Tsuyoshi Nakaya[1] **and Robert K Plunkett**[2,3]

[1] Kyoto University, Department of Physics, Kyoto 606-8502, Japan
[2] Fermi National Accelerator Laboratory, Batavia, IL 60510, USA
[3] Author to whom any correspondence should be addressed.

E-mail: t.nakaya@scphys.kyoto-u.ac.jp **and** plunk@fnal.gov

Keywords: neutrino, particle physics, oscillations

Abstract

This paper discusses recent results and near-term prospects of the long-baseline neutrino experiments MINOS, MINOS+, T2K and NOvA. The non-zero value of the third neutrino mixing angle θ_{13} allows experimental analysis in a manner which explicitly exhibits appearance and disappearance dependencies on additional parameters associated with mass-hierarchy, CP violation, and any non-maximal θ_{23}. These current and near-future experiments begin the era of precision accelerator long-baseline measurements and lay the framework within which future experimental results will be interpreted.

1. Introduction to long-baseline accelerator experiments

1.1. Motivation and three-flavor model

Beginning with the successful operation of the K2K experiment [1], the physics community has seen a profound expansion of our knowledge of the mixing of neutrinos, driven by long-baseline accelerator experiments [2–6], experiments studying atmospheric neutrinos [7–9], solar neutrinos [10], and, most recently, high-precision experiments with reactor neutrinos [11]. In this article we describe the current generation of the running long-baseline neutrino experiments T2K and MINOS/MINOS+ , and the status of the NOvA experiment which was commissioned in 2014. Each of these experiments was designed with primary and secondary goals. For example, MINOS had as its principle justification the measurement, via disappearance of ν_μ, of the mixing parameters $\sin^2\theta_{23}$ and Δm^2_{32}, with particular emphasis on Δm^2_{32}. T2K and NOvA were primarily designed to elucidate the structure of the neutrino sector by studies of ν_e appearance. However they are making and will continue to make very significant contributions to the study of ν_μ disappearance as well. Similarly, MINOS has measured ν_e appearance and the angle θ_{13}.

This situation leads us to a point we will emphasize throughout this article, namely that the traditional distinction between various modes of study of mixing, matter effects, and CP violation is rapidly giving way to a more integrated approach which utilizes both major types of signals to gain maximal information about the somewhat complicated three-neutrino sector. We will first discuss the relevant formalism and the major measurements required to test it. Next we will provide a technical overview of the powerful neutrino beams required for the measurements, and then proceed to discuss the experiments together with their current measurements and expected sensitivities. Finally, we conclude the article with a discussion of the near-term future for these experiments.

It is our goal to familiarize the reader with the surprisingly rich information already available in studies of this sector of physics, the only one currently not well-handled by the Standard Model. In addition, we will provide context for future discussions of progress to be provided by these experiments and by the exciting future world of very large experiments, and very long baselines.

1.2. Core measurements

In the three-neutrino model there is a close relationship among the disappearance and appearance modes of oscillation study, going back to their origin in the PMNS matrix. Following reference [12], it is possible to write the disappearance possibility for muon neutrinos in vacuum, as

$$P(\nu_\mu \to \nu_\mu) = 1 - 4\sin^2\theta_{23}\cos^2\theta_{13}\left(1 - \sin^2\theta_{23}\cos^2\theta_{13}\right)\sin^2\frac{\Delta m^2_{\rm eff}L}{4E}, \quad (1)$$

where $\Delta m^2_{\rm eff}$ incorporates effective leading dependences on the additional PMNS parameters Δm^2_{21}, θ_{13}, and $\delta_{\rm CP}$ as

$$\Delta m^2_{\rm eff} = \Delta m^2_{32} + \Delta m^2_{21}\sin^2\theta_{12} + \Delta m^2_{21}\cos\delta_{\rm CP}\sin\theta_{13}\tan\theta_{23}\sin 2\theta_{12}.$$

Equation (1) may be simply manipulated to yield a form appropriate for the baseline of the T2K experiment, namely

$$P(\nu_\mu \to \nu_\mu) \simeq 1 - \left(\cos^4\theta_{13}\sin^2 2\theta_{23} + \sin^2 2\theta_{13}\sin^2\theta_{23}\right)\sin^2\frac{\Delta m^2_{31}L}{4E}. \quad (2)$$

Here we see the vital role of the mixing angle θ_{13}, which couples in the PMNS matrix to the CP-violating phase $\delta_{\rm CP}$. It is now well-known that this angle is relatively large, approximately 9° [10]. T2K, MINOS/MINOS +, and future NOvA measurements of this angle and its consequences are discussed in sections 3, 4 and 7.

Because the Earth between the beam creation point and the detector location forms an essential part of any long-baseline experiment, its effects on the measurements must be considered. This creates both problems and opportunities—problems because of the introduction of degeneracies between matter effects and CP violation, and opportunities because of the possibilities to exploit the differences between neutrino and antineutrino interactions, and from the two mass hierarchies.

1.2.1. Appearance measurements and $\sin^2 2\theta_{13}$

A large value of θ_{13} is key to allowing an integrated approach to oscillation studies. MINOS, T2K, and soon NOvA use the appearance channel for ν_e with a muon neutrino beam to probe θ_{13} directly. In appropriate approximation for a muon neutrino with energy E_ν of $O(1)$ GeV traveling a distance of $O(100)$ km, the leading order equation governing the appearance probability is:

$$P(\nu_\mu \to \nu_e) \approx \sin^2\theta_{23}\sin^2 2\theta_{13}\sin^2\frac{\Delta m^2_{32}L}{4E}. \quad (3)$$

Equation (3) is applicable for both neutrino and anti-neutrino oscillations.

The difference between neutrinos and anti-neutrinos in oscillation appears as a sub-leading effect, including the solar parameters θ_{12} and Δm^2_{21} and CP violation phase $\delta_{\rm CP}$. The probability is expressed [13, 14] as

$$P(\nu_\mu \to \nu_e) \simeq \sin^2 2\theta_{13}T_1 - \alpha\sin 2\theta_{13}T_2 + \alpha\sin 2\theta_{13}T_3 + \alpha^4 T_4, \quad (4)$$

where $\alpha \equiv \dfrac{\Delta m^2_{21}}{\Delta m^2_{31}}$ is the small ($\sim$1/30) ratio between the solar and atmospheric squared-mass splittings, and

$$T_1 = \sin^2\theta_{23}\frac{\sin^2[(1-A)\Delta]}{\left(1-A^2\right)},$$

$$T_2 = \sin\delta_{\rm CP}\sin 2\theta_{12}\sin 2\theta_{23}\sin\Delta\frac{\sin(A\Delta)}{A}\frac{\sin[(1-A)\Delta]}{1-A},$$

$$T_3 = \cos\delta_{\rm CP}\sin 2\theta_{12}\sin 2\theta_{23}\cos\Delta\frac{\sin(A\Delta)}{A}\frac{\sin[(1-A)\Delta]}{1-A},$$

$$T_4 = \cos^2\theta_{23}\sin^2 2\theta_{12}\frac{\sin^2(A\Delta)}{A^2}.$$

Here, $\Delta = \dfrac{\Delta m^2_{32}L}{4E_\nu}$ and $A \equiv 2\sqrt{2}\,G_F n_e E_\nu/\Delta m^2_{32}$, where N_e is the electron density of Earth's crust. In equation (4), the sign of the second term changes for anti-neutrinos, governing CP violation when all three mixing angles, including θ_{13}, have nonzero values. With current best knowledge of oscillation parameters, the CP violation (sub-leading term) can be as large as $\sim$30% of the leading term.

The A dependence arises from matter effects (caused by additional terms in the Hamiltonian for the electron component of the neutrino eigenstate), which are coupled with the sign of Δm^2_{32}. In this paper, we refer to $\Delta m^2_{32} > 0$ as the normal mass hierarchy and $\Delta m^2_{32} < 0$ as the inverted one.

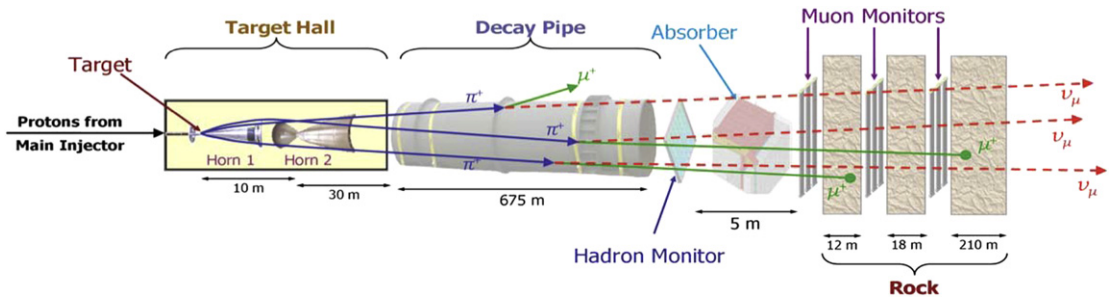

Figure 1. Layout of the NuMI beamline at Fermilab, showing main components of the target, focusing, and decay systems [15].

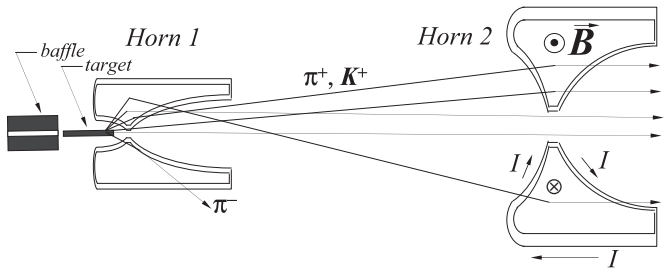

Figure 2. Detail of the magnetic focusing horn system for the NuMI beam line [16].

1.2.2. Hierarchy, octants, and CP violation (δ_{CP})
The subleading terms shown in equations (1) and (4) make it possible in principle for oscillation measurements to be sensitive to the octant of θ_{23} ($\theta_{23} < \pi/4$ or $\theta_{23} > \pi/4$), in the case it is not maximal (i.e. $= \pi/4$). Even for maximal mixing, the additional dependencies in equation (4), and further terms added to equation (2) enable the combination of disappearance and appearance results to begin to give clues to the CP and hierarchy puzzles.

2. Beamlines

2.1. NuMI

The conceptual beginning of the NuMI beamline dates to the era of the construction of the Fermilab main injector. The beamline, together with its associated tunnels, experimental halls, surface buildings and infrastructure, was built between 1999 and 2004. Datataking with the beam began in March of 2005, and continues to this time. The complex currently consists of a primary beam transport, the NuMI target hall, a 675 meter He-filled decay pipe of one meter radius, a hadron absorber and muon flux monitor area, meters of rock shielding, and two experimental halls—the first housing the MINOS near detector and the MINERvA detector, and the second housing the NOvA near detector. Figure 1 shows the general configuration of the beamline.

Beam from the Fermilab Booster is accelerated in the Main Injector to 120 GeV, and then extracted with a system of fast kickers. As part of an upgrade to beam power, commissioning is underway to stack beam in the Fermilab recycler ring before transfer to the main injector. At the NuMI target the proton beam consists of six batches, with a total extraction period of 10 μs. The time between extractions has varied from 2.2 s to the current 1.3 s. This low duty factor allows the MINOS and NOvA experiments to trigger on a simple timing window, which facilitates the surface location of the NOvA far detector. Overlaying multiple injections from the booster in the main injector (slip-stacking) has allowed the beam intensity to reach 375 kW. The NuMI beam for NOvA is anticipated to reach 700 kW, with a similar time structure.

Secondary hadrons created in the interaction of the extracted proton beam with a 94 cm graphite target are focused by a system of two magnetic horns. Historically, the focused hadron momentum (which translates into neutrino energy) has been adjustable by moving the target w.r.t the first horn. This is more difficult in the NOvA beam configuration, which is optimized for the off-axis application. Figure 2 shows the focusing schema of the NuMI beam.The majority of the data samples used in MINOS physics analyzes have used the NuMI beam line focused at its lowest practical energy configuration, with a peak neutrino energy at approximately 3 GeV. Additional samples at higher neutrino beam energy settings have been used to provide information on the

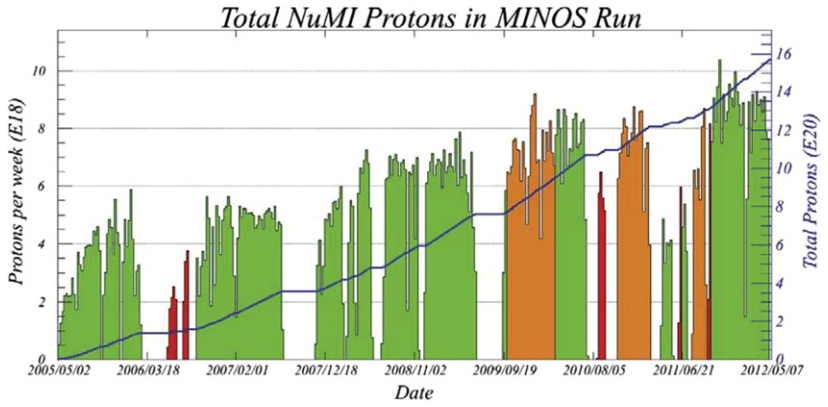

Figure 3. Total NuMI beam delivery during MINOS running. The total collected in the principle neutrino configuration was 10.7×10^{20} protons. For the antineutrino configuration the total was 3.4×10^{20} protons.

intrinsic ν_e component of the beam, an important and irreducible background for the measurement of $\sin^2 2\theta_{13}$. Overall beam production for the MINOS running period 2005–2012, is shown in figure 3.

An important feature of horn-focused beamlines like the NuMI beamline is the ability to convert from focusing positive hadrons (primarily π^+) to negative hadrons (primarily π^-), which creates a beam heavily enriched in antineutrinos. Using this beam, MINOS has published special studies of the oscillation parameters of $\bar{\nu}_\mu$ [17].

Targetry which can withstand the repeated high power proton pulses needed for a neutrino beam represents a technical challenge. The NuMI targets used for MINOS data taking were constructed of 47 segmented graphite fins. A total of seven targets were used in the period 2005 to 2012, with exchanges usually due to failures in auxiliary cooling systems. In one case the target material experienced significant degradation, visible in the produced neutrino rates. Significant engineering changes have occurred for the targets to be used in the NOvA beam, which must withstand 700 kW operations. These include detailed changes to the graphite fins to allow for an increase in primary beam spot size from 1.1 to 1.3 mm, and, importantly, a significant relocation of the water cooling tubing to decrease its vulnerability. With these changes, it is expected that the NuMI targets in the NOvA era will survive a minimum of a year of high power operation before any replacement is needed.

2.2. Off axis neutrino beam (OAB)

An OAB configuration [18] is a method to produce a narrow band energy neutrino beam. In the OAB configuration, the axis of the beam optics is intentionally shifted by a few degrees from the detector direction. With a finite decay angle, the neutrino energy becomes almost independent of the parent pion energy due to characteristics of the two body decay kinematics of the pion with Lorentz boost.

The off-axis beam principle can be illustrated with a simple algebraic example. Let us model the beam as consisting of pions which are fully focused in the on-axis directions. The transverse and perpendicular components of the decay neutrino momentum obey the relations:

$$P_T = P^* \sin\theta^*,\ P_L = \gamma P^* \left(1 + \cos\theta^*\right) \approx E_{\nu,} \tag{5}$$

where P^* and θ^* are the decay momentum and angle in the rest frame of the decaying particle. The fixed off-axis angle condition is $\theta_{\rm lab} = P_T/P_L$.

Near $\theta^* = \pi/2$, we have $\Delta P_T \approx 0$ for variations in θ^*, and therefore

$$\Delta P_L = \frac{\Delta P_T}{\theta_{\rm lab}} \approx 0. \tag{6}$$

Physically, the constraint on the angle means that the variation of neutrino energy that normally occurs when θ^* varies is greatly reduced, and parent particles of many energies contribute to a single peak in neutrino energy. As a consequence, the peak energy of the neutrino beam depends on the off-axis angle. Figure 5 illustrates this effect graphically for several off-axis angles in the NuMI configuration.

By changing the off axis angle, it is possible to tune the neutrino beam energy to maximize the sensitivity of the oscillation parameters. As a reference, the off axis angle can be varied from 2.5° to 3.0° in the T2K beamline, which corresponds to a mean energy of neutrinos in the range from 0.5 to 0.9 GeV.

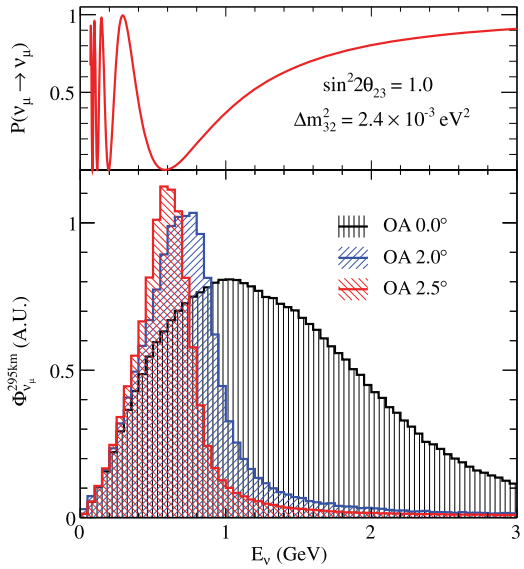

Figure 4. The neutrino oscillation probability of $\nu_\mu \to \nu_\mu$ and the neutrino energy spectrum with different off-axis angles in T2K from [19].

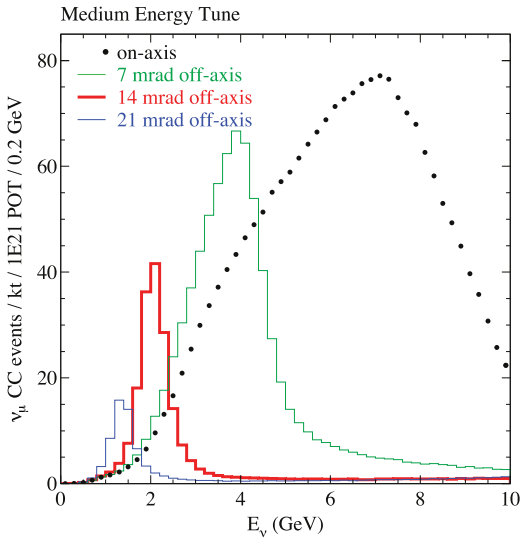

Figure 5. The neutrino spectra (flux times cross-section) for various angles in a medium-energy NuMI beam [20].

The neutrino energy spectra at the far detector (Super-Kamiokande) with different off-axis angles in T2K are shown in figure 4 [19]. In T2K, the off-axis angle is set to 2.5°.

The NOvA experiment is situated at an off-axis angle of 14 mrad (0.8°). With a higher beam energy focusing than used for the MINOS program, this results in a large flux at the neutrino energy associated with oscillations. At the same time, it reduces backgrounds from neutral current (NC) interactions from higher energies and from intrinsic beam ν_e, which have a wider energy distribution.

2.3. T2K neutrino beam

J-PARC, the Japan Proton Accelerator Research Complex, is the accelerator complex supplying 30 GeV protons to the T2K experiment. An intense neutrino beam with a narrow-band energy spectrum is produced using the off-axis technique. The beam energy is tuned to the oscillation maximum (~600 MeV for the T2K baseline of 295 km), which also suppresses the high energy component contributing to background generation. The left plot in figure 6 shows the prediction of the T2K neutrino beam flux at the far detector, Super-Kamiokande (Super-K). The flux is dominated by muon neutrinos with a small fraction (at the level of a few %) of intrinsic

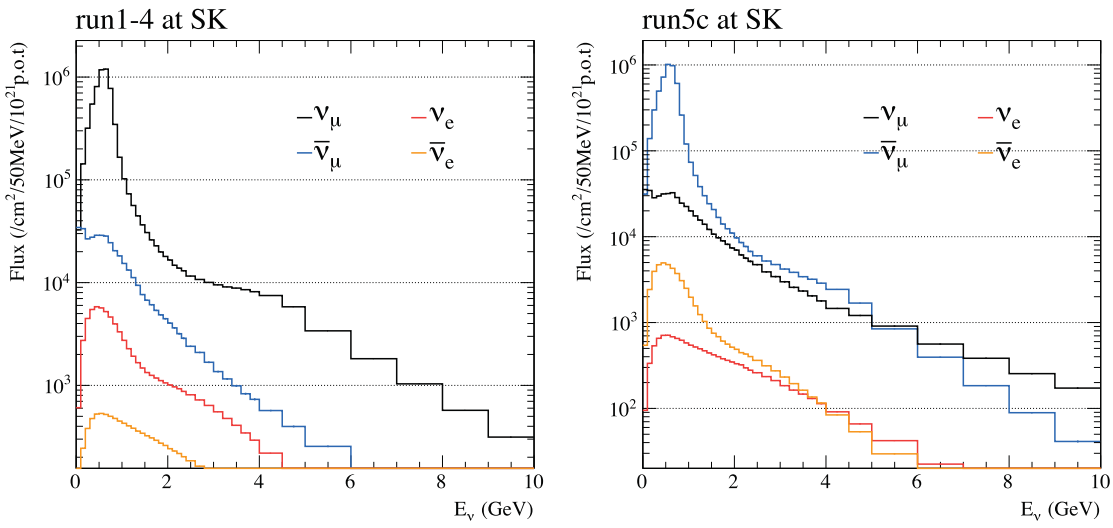

Figure 6. Prediction of the T2K beam flux for neutrinos and antineutrinos at Super-K. The left plot is for the neutrino beam mode made by focusing the positively charged particles, and the right is for the anti-neutrino mode made by focusing the negative ones. The flux above $E_\nu = 10$ GeV is not shown although the flux is simulated up to $E_\nu = 30$ GeV.

electron neutrinos, referred to as 'beam ν_e'. The beam ν_e component is a major background when searching for electron neutrino appearance.

The proton beam is directed onto a graphite target which is designed to accept 750 kW beam power. The target is a graphite rod of 91.4 cm long and 2.6 diameter with 1.8 g cm^{-3} density. The target is helium-cooled. Since the current beam power is still around 350 kW, there is still a margin for safety. The details of the T2K target are found in [21]. The positively charged particles (mainly pions) produced are focused by three magnetic horns, typically operated at 250 kA. The decay of the charged particles in a 100 m decay volume produces the neutrino beam. By reversing the direction of the horn current, negatively charged particles are focused to produce the anti-neutrino beam. The prediction of the anti-neutrino beam flux is shown at the right plot in figure 6. Thanks to the off-axis technique, the signal to noise ratio of the anti-neutrino beam flux is as good as 30 [4] at the flux peak, while the wrong sign component of neutrinos is broadly distributed in energy.

T2K started physics data taking in January 2010. Although the data taking was interrupted on March 11, 2011 by the Great East Japan Earthquake, the experiment collected 6.57×10^{20} protons on target (POT) for analysis before May 2013[5]. The history of data taking is shown in figure 7. In 2014, anti-neutrino beam running began. Today, a maximum beam power of 370 kW has been recorded in J-PARC.

3. Electron appearance analysis

3.1. MINOS

The MINOS experiment, with its magnetized steel calorimeters, was principally designed to detect and classify the charged–current (CC) reactions $\nu_\mu + N \rightarrow \mu^- + X$ and $\bar{\nu}_\mu + N \rightarrow \mu^+ + X$. In order to detect and measure the appearance of ν_e and $\bar{\nu_e}$, which indicate a non-zero θ_{13}, sophisticated statistical techniques must be used to disentangle the relative contributions of this signal from the similar NC background. To do this, MINOS uses the library event matching (LEM) technique [22]. This procedure uses large ($> 10^7$) simulated samples of signal and background events to form event-by-event comparisons of the observed deposited charge in detector channels with the equivalent simulated deposited charge in the library events. The LEM procedure gives a set of output variables which are used as input to a simple artificial neural net, giving a statistical discriminant ($\alpha_{\rm LEM}$), which can be used to identify signal and background components of the data.

The discriminant $\alpha_{\rm LEM}$ is formed by the output of a neural net which has been given as inputs the reconstructed event energy and characteristics of the 50 best-matched library events, namely (i) the fraction of these library events that are nue CC events, (ii) their average inelasticity (y) and (iii) the average overlapping fraction of charge on strips between the data and the 50 library events. Events with $\alpha_{\rm LEM} > 0.6$ are selected for further analysis.

[4] The signal to noise ratio of anti-neutrinos to neutrinos is typically much worse than that of neutrinos to anti-neutrinos.

[5] J-PARC stopped operation in May 2013 because of the hadron hall accident.

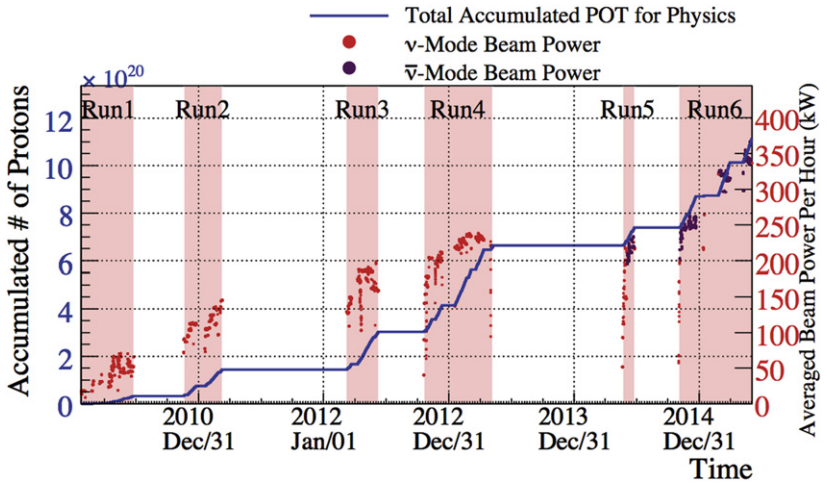

Figure 7. The history of the delivered protons to the T2K experiment for analysis. The dots show the number of protons per pulse, and the lines show the integrated number of protons. The red dots are for the neutrino beam running, and the purple dots are for the anti-neutrinos.

Next, to search for appearance of ν_e due to the oscillation phenomenon, the spectra of the varying background components present in the beam (ν_μ-CC, NC, and residual beam ν_e-CC) need to be estimated using data from the near detector. This is done in MINOS by comparing samples obtained from different beam focusing configurations for decaying secondaries, as discussed in [23]. Figure 8, from [5] shows the far detector MINOS data and the expected backgrounds, for various bins of α_{LEM}.

The final elements required to produce an appearance measurement are extrapolation of the background (and oscillated signal) estimates between near and far detectors, and an estimate of the signal efficiency. The first is done by comparison of the background measured in the ND with its simulated value, giving a correction factor that can be applied to the equivalent simulation of the far detector. The technique is simpler than that used for MINOS CC appearance measurement; however the essential equivalence of the methods has been demonstrated in [16]. In order to estimate the signal efficiency, hybrid events were created by substitution of a simulated electron shower in shower-subtracted, well-identified CC events. The efficiencies obtained were $> 55\%$ in both beam configurations.

The principal systematic errors affect the result are uncertainties in the background estimation and in the signal efficiency. They are 3.8% (4.8%) and 2.8% (3.1%), respectively, for the ν ($\bar{\nu}$) modes. The measurement is dominated by statistical errors, affecting both the signal and the background estimation. MINOS systematic errors are discussed further in section 5.3.

After establishment of these techniques and their systematic errors, MINOS can now use the near detector spectrum to extrapolate the expectation of signal and background for hypothesized values of the the physical parameters θ_{13}, δ_{CP}, and mass hierarchy, to determine statistically allowed and disallowed regions. The overall background estimation for the ν beam configuration is 127.7 background events. For parameter values of $\sin^2 2\theta_{13} = 0.1, \delta_{\mathrm{CP}} = 0, \theta_{23} = \pi/4$ and normal hierarchy, 33.7 ± 1.9 appearance events are expected, giving a signal/background ratio of $S/B = 0.26$. A total of 152 events are observed. Contributions to the analysis from the $\bar{\nu}$ beam configuration are small, totaling only 21.4 expected and 20 observed events. The result from [5] is shown in figure 9 for the full MINOS dataset, consisting of 10.6×10^{20} POT for the ν beam configuration and 3.3×10^{20} POT for the $\bar{\nu}$ beam configuration. This analysis does not distinguish between neutrinos and antineutrinos. The result shows the characteristic features of periodic variation with δ_{CP}, as well as shape inversion with hierarchy choice. MINOS cites best-fit values for $2\ \sin^2 2\theta_{13}\ \sin^2\theta_{23}$ of $0.051^{+0.038}_{-0.030}$ under the normal hierarchy assumption, and $0.093^{+0.052}_{-0.049}$ for the inverted hierarchy, with 90% confidence ranges of 0.01–0.12 and 0.03–0.18 , respectively. The best fits are all computed for $\delta_{\mathrm{CP}} = 0$, and $\theta_{23} < \pi/4$.

It is of interest to examine the parameter space probed by this appearance analysis more closely. The MINOS collaboration has computed the change in likelihood for excursions of the CP-violating phase δ_{CP} for four combinations of the hierarchy and θ_{23} octant parameters. This result from [5] is shown in figure 10. The experiment disfavors 31% of the total three-parameter space (δ_{CP}, hierarchy, octant) at 68%C.L. and shows a suggestive, but statistically limited preference for the inverted mass hierarchy scenario.

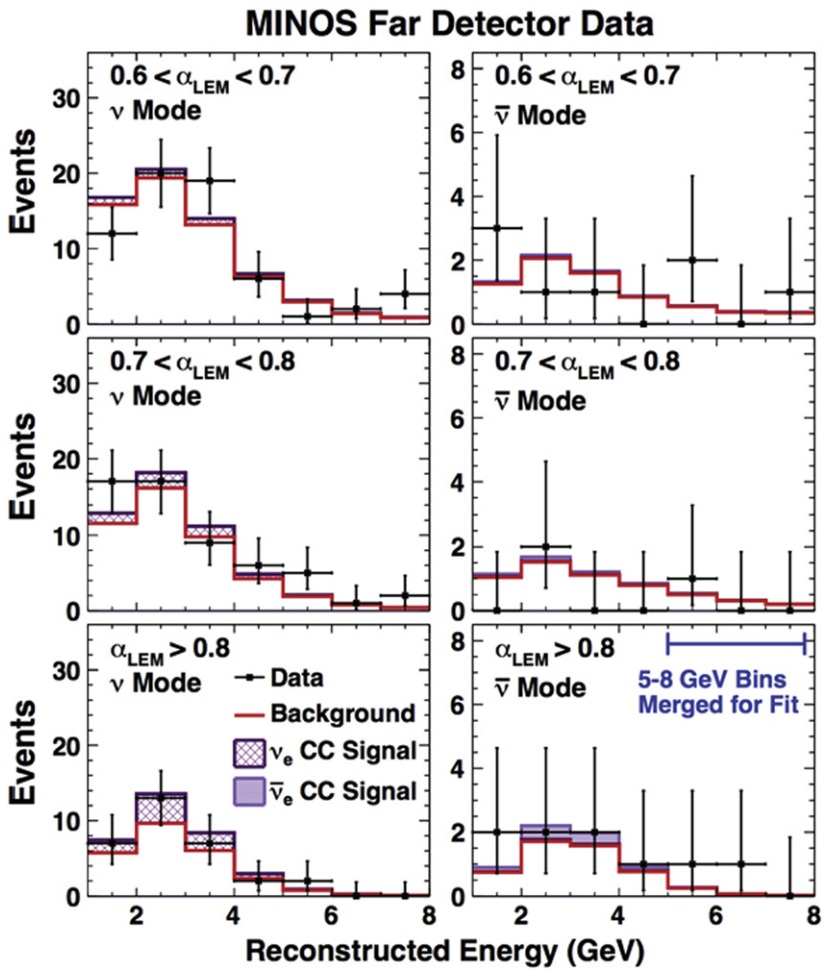

Figure 8. MINOS far detector data with statistical errors [5] used for ν_e appearance analysis, compared with expectations for $\sin^2(2\theta_{13}) = 0.051$, $\Delta m^2_{32} > 0$, $\delta = 0$, and $\theta_{23} = \pi/4$.

3.2. T2K

The first evidence of non-zero θ_{13} was reported [22, 24] in the $\nu_\mu \rightarrow \nu_e$ appearance channel in 2011. Today, with more data collected in T2K, the $\nu_\mu \rightarrow \nu_e$ transition is well established [3]. Twenty-eight electron candidate events in T2K have been observed in the T2K far detector (Super-K) by requiring one Cherenkov 'ring', identified as an electron type with visible energy greater than 100 MeV. In addition, a newly developed algorithm was applied to suppress background events with a $\pi^0 \rightarrow 2\gamma$, where one of the photons is missed in reconstruction. The details of event selection are found in [3, 25]. The number of observed events, compared with the expectations is shown in table 1. The observed number of events, 28, is significantly larger than the expected number, 4.92 ± 0.55, with $\theta_{13} = 0$, but is consistent with the expectation of 21.6 with $\sin^2 2\theta_{13} = 0.10$ and $\delta_{CP} = 0$.

The best fit value of θ_{13} has been evaluated to be $\sin^2 2\theta_{13} = 0.140 \pm 0.038 (0.170 \pm 0.045)$ for the normal (inverted) hierarchy case with a 68% confidence level (C. L.), by fixing the other oscillation parameters: $\sin^2 2\theta_{12} = 0.306$, $\Delta m_{21} = 7.6 \times 10^{-5}$ eV^2, $\sin^2 \theta_{23} = 0.5$, $|\Delta m^2_{32}| = 2.4 \times 10^{-3}$ eV^2, and $\delta_{CP} = 0$. Figure 11 shows the electron momentum versus angle distribution (sensitive to the oscillation), which is used to extract the oscillation parameters $\sin^2 2\theta_{13}$ and δ_{CP} which give the best fit values. The significance for a nonzero θ_{13} is calculated to be 7.3 σ.

Allowed regions for $\sin^2 2\theta_{13}$ as a function of δ_{CP} are evaluated as shown in figure 12, where the values of $\sin^2\theta_{23}$ and Δm^2_{32} are varied in the fit with additional constraints from [26]. In order to be sensitive to δ_{CP}, T2K uses the value of θ_{13}, 0.098 ± 0.013, from reactor experiments in PDG2012 [10]. The $-2\Delta \ln L$ in the fit as a function of δ_{CP} is extracted, and is shown in figure 13. The T2K measurement, together with the reactor θ_{13} value prefers $\delta_{CP} = -\pi/2$ with an exclusion of $0.19\pi < \delta_{CP} < 0.80\pi$ ($-\pi < \delta_{CP} < -0.97\pi$ and $-0.04\pi < \delta_{CP} < \pi$) with normal (inverted) hierarchy at 90% C.L. This may be a hint of CP violation in neutrinos.

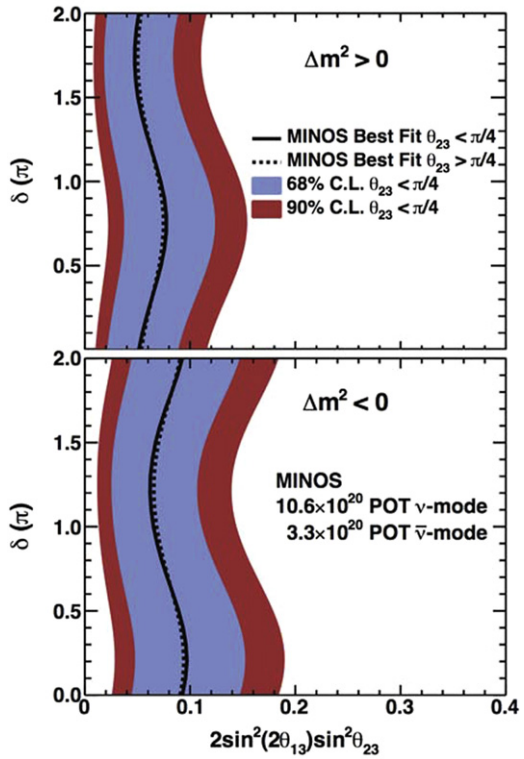

Figure 9. MINOS allowed contours at 68% and 90% confidence for the measured quantity $2\sin^2 2\theta_{13}\sin^2\theta_{23}$, as a function of δ_{CP}. Systematic and statistical uncertainties are included, and results for both assumed hierarchies are displayed.

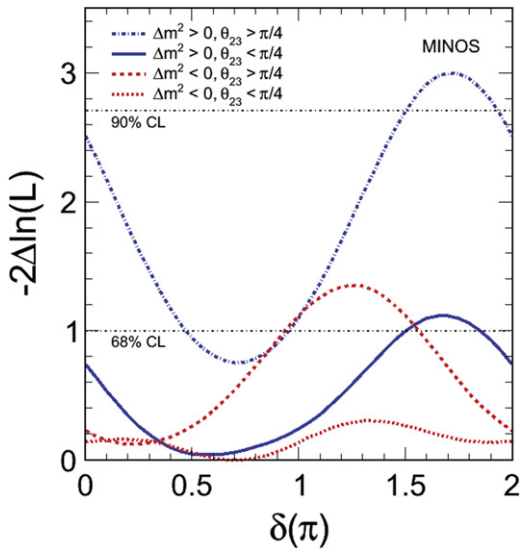

Figure 10. Variation of likelihood (compared to best fits) with δ_{CP}, plotted as $-2\Delta\ln(L)$, for the observed ν_e appearance in MINOS, shown for varying combinations of other oscillation parameters. Values above the horizontal dashed lines are disfavored at either 68% or 90% C. L.

Table 1. The number of observed events with the MC expectations and efficiencies. The oscillation parameters are assumed to be $\sin^2 2\theta_{13} = 0.1$, $\sin^2\theta_{23} = 0.5$, $|\Delta m^2_{32}| = 2.4 \times 10^{-3}$ eV^2, $\delta_{CP} = 0$, and $\Delta m^2_{32} > 0$

	Data	Total MC	Signal $\nu_\mu \to \nu_e$ CC	$\nu_\mu + \overline{\nu}_\mu$ CC	Beam $\nu_e + \overline{\nu}_e$ CC	NC
ν_e events	28	21.6	17.3	0.1	3.2	1.0
Efficiency (%)	—	—	61.2	0.0	19.1	0.4

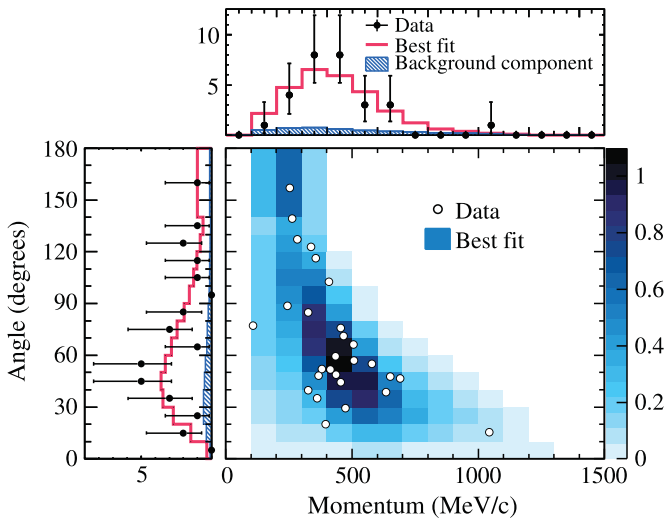

Figure 11. The T2K electron momentum versus angle distribution for 28 single-ring electron events, together with the MC expectation in [3]. The best fit value of $\sin^2 2\theta_{13} = 0.140$ in the normal hierarchy case is used for the expectation.

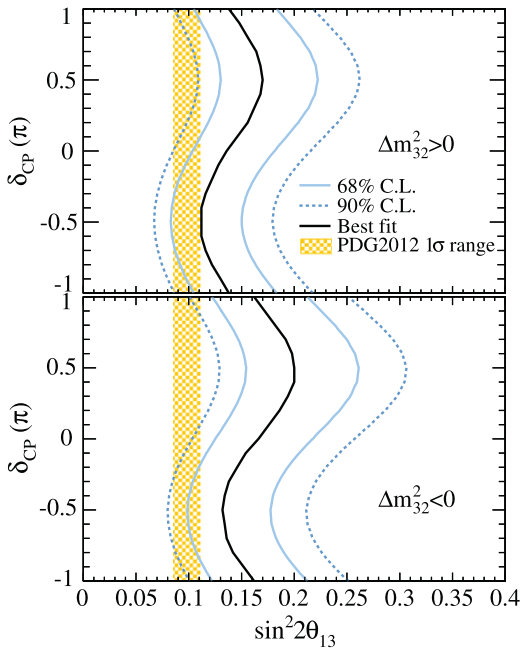

Figure 12. The allowed regions for $\sin^2 2\theta_{13}$ as a function of δ_{CP} for the normal mass hierarchy case (top) and the inverted one (bottom) from [3]. The value of θ_{13} from reactor experiments in PDG2012 is shown as the shaded region.

4. Precise measurements of oscillation parameters

4.1. T2K ν_μ disappearance analysis

The most precise measurement of θ_{23} has been carried out [2] by T2K based on the data set of 6.57×10^{20} POT. First, a single-ring muon sample[6] is selected by requiring one muon-type Cherenkov ring with momentum greater than 200 MeV/c in Super-K. The details of the event selection are found in [2]. One hundred twenty events are selected while the expectation without neutrino oscillation is 446.0 ± 22.5 (syst.). The neutrino energy for each event is calculated under the quasi-elastic (QE) assumption using the expression

[6] The number of rings corresponds to the number of observed particles in Super-K.

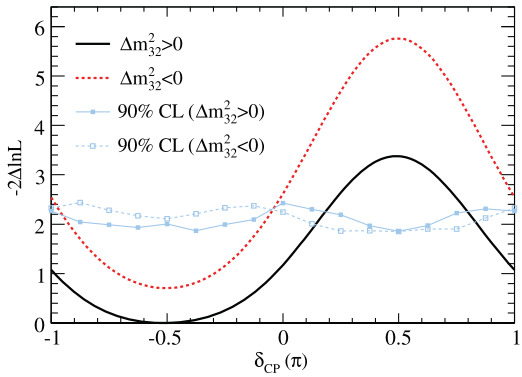

Figure 13. The $-2\Delta \ln L$ value as a function of δ_{CP} with the reactor θ_{13} constraints for normal and inverted hierarchies from [3]. The likelihood is marginalized over θ_{13}, θ_{23} and Δm^2_{32}. The 90% C.L. is evaluated by using the Feldman–Cousins method. The δ_{CP} regions with values above the 90% C.L. lines are excluded.

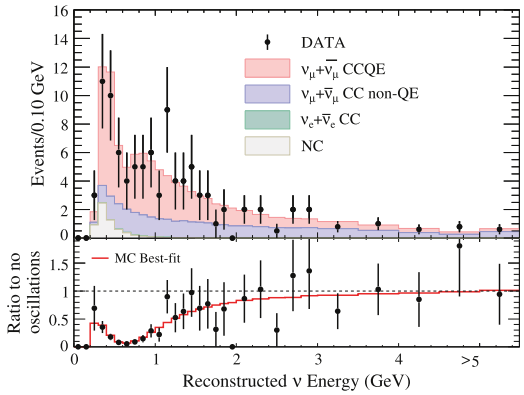

Figure 14. The neutrino energy spectrum for single-ring muon events in [2]. (Top) The observed and expected spectra with the event categories in the simulation. (Bottom) The ratio of the observed spectrum to the no-oscillation hypothesis with the best-fit case.

$$E_\nu^{\rm rec} = \frac{m_{\rm p}^2 - \left(m_{\rm n} - E_{\rm b}\right)^2 - m_{\rm l}^2 + 2\left(m_{\rm n} - E_{\rm b}\right)E_{\rm l}}{2\left(m_{\rm n} - E_{\rm b} - El + p_{\rm l}\cos\theta_{\rm l}\right)}, \tag{7}$$

where $m_{\rm p}$ is the proton mass, $m_{\rm n}$ the neutron mass, $m_{\rm l}$ the lepton mass, $E_{\rm l}$ the lepton energy, and $E_{\rm b} = 27$ MeV the binding energy of a nucleon inside a ^{16}O nucleus. Figure 14 shows the neutrino energy of the observed 120 events with the MC expectations for neutrino oscillations.

Using the number of events and the neutrino energy spectrum, the oscillation parameters ($\sin^2\theta_{23}$, $\Delta m^2_{32(13)}$) are estimated with an un-binned maximum likelihood fit for the normal (inverted) mass hierarchies. Details of the method are found in [2]. The result is shown in figure 15.

The best fit value with the 1D 68% confidence intervals are $\sin^2\theta_{23} = 0.514^{+0.055}_{-0.056}$ (0.511 ± 0.055) and $\Delta m^2_{32} = 2.51 \pm 0.10$ ($\Delta m^2_{13} = 2.48 \pm 0.10$) $\times 10^{-3}$eV^2 for the normal (inverted) hierarchy case. The result is consistent with the maximal possible disappearance probability and is more precise than previous measurements, especially for $\sin^2\theta_{23}$.

4.2. Joint analysis of ν_μ disappearance and ν_e appearance samples in MINOS

Beginning in 2005 (2003 for collection of atmospheric data), the MINOS experiment has provided precision measurements of the oscillation parameters Δm^2 and $\sin^2(2\theta)$ for effective definitions of these parameters in a two-neutrino approximation. Most recently, MINOS has quoted $2.28 \times 10^{-3} < |\Delta m^2_{32}| < 2.46 \times 10^{-3}$ eV^2 (68% confidence) and a 90% C.L. range for θ_{23} of $0.37 < \sin^2\theta_{13} < 0.64$ (both normal mass hierarchy), using a complete three-neutrino description of the data [6]. Atmospheric data and appearance data are included in the combined fits. In particular, the ν_e appearance data and atmospheric data provide, in principle, sensitivity to additional information concerning mass hierarchy and CP phase. As an example, the atmospheric data sample, divided into neutrino and antineutrino samples for up-going multi-GeV events, shows different matter effects for normal and inverted hierarchies. In the current sample, these additional sensitivities are limited, as shown by

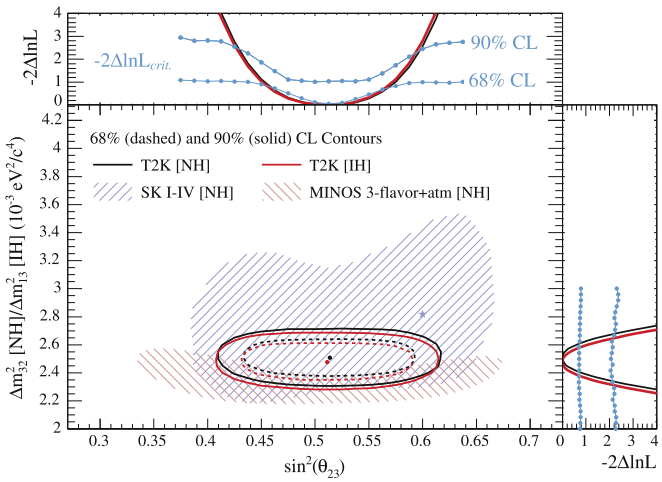

Figure 15. T2K Contours of oscillation parameters $\sin^2\theta_{23}$ versus $|\Delta m^2_{32(13)}|$ for 68% and 90% C.L. region. The one-dimensional profile likelihoods are also shown for each oscillation parameter in the top and right windows. The 1D $-2\Delta \ln L_{\text{critical}}$ values for the normal mass hierarchy are shown in the windows. The Super-Kamiokande [27] and MINOS [6] results are also shown for comparison.

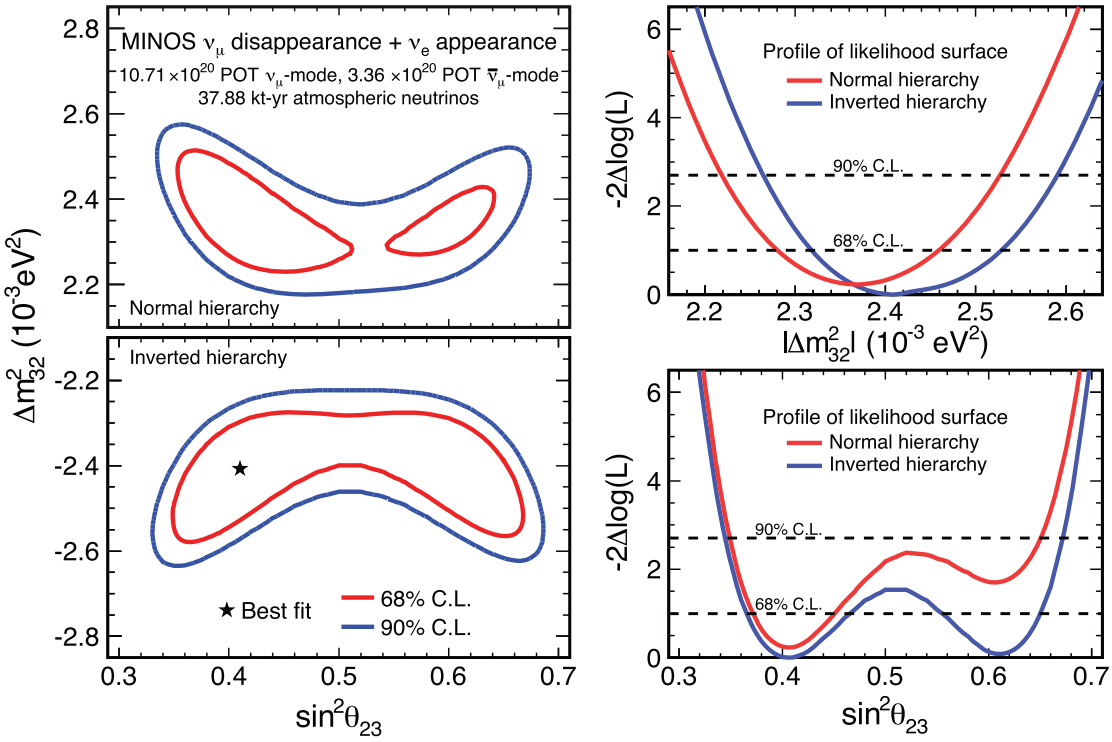

Figure 16. MINOS three-flavor oscillation parameters using both disappearance and appearance data. Left: confidence level contours for assumed normal and inverted hierarchies, computed using $-2\Delta \ln(L)$ w.r.t. the overall best fit point (star). Right: one-dimensional likelihood profiles for the parameters. All results from [6].

the presentation in figure 16, and the fitted values of $|\Delta m^2_{32}|$ and $\sin^2\theta_{23}$ are consistent [6]. The fit results are obtained using constraints from external data. In particular, a value of $\sin^2\theta_{13} = 0.0242 \pm 0.0025$ has been taken from a weighted average of reactor experiment values [11], and solar oscillation parameters are taken from [28].

4.3. Joint analysis of ν_μ disappearance and ν_e appearance samples in T2K

The oscillation probability of $\nu_\mu \rightarrow \nu_e$ depends on many oscillation parameters: $\sin^2\theta_{13}$, $\sin^2\theta_{23}$, Δm^2_{32} and δ_{CP}; that of $\nu_\mu \rightarrow \nu_\mu$ depends mainly on $\sin^2\theta_{23}$ and Δm^2_{32}. Therefore, all oscillation parameters can be efficiently

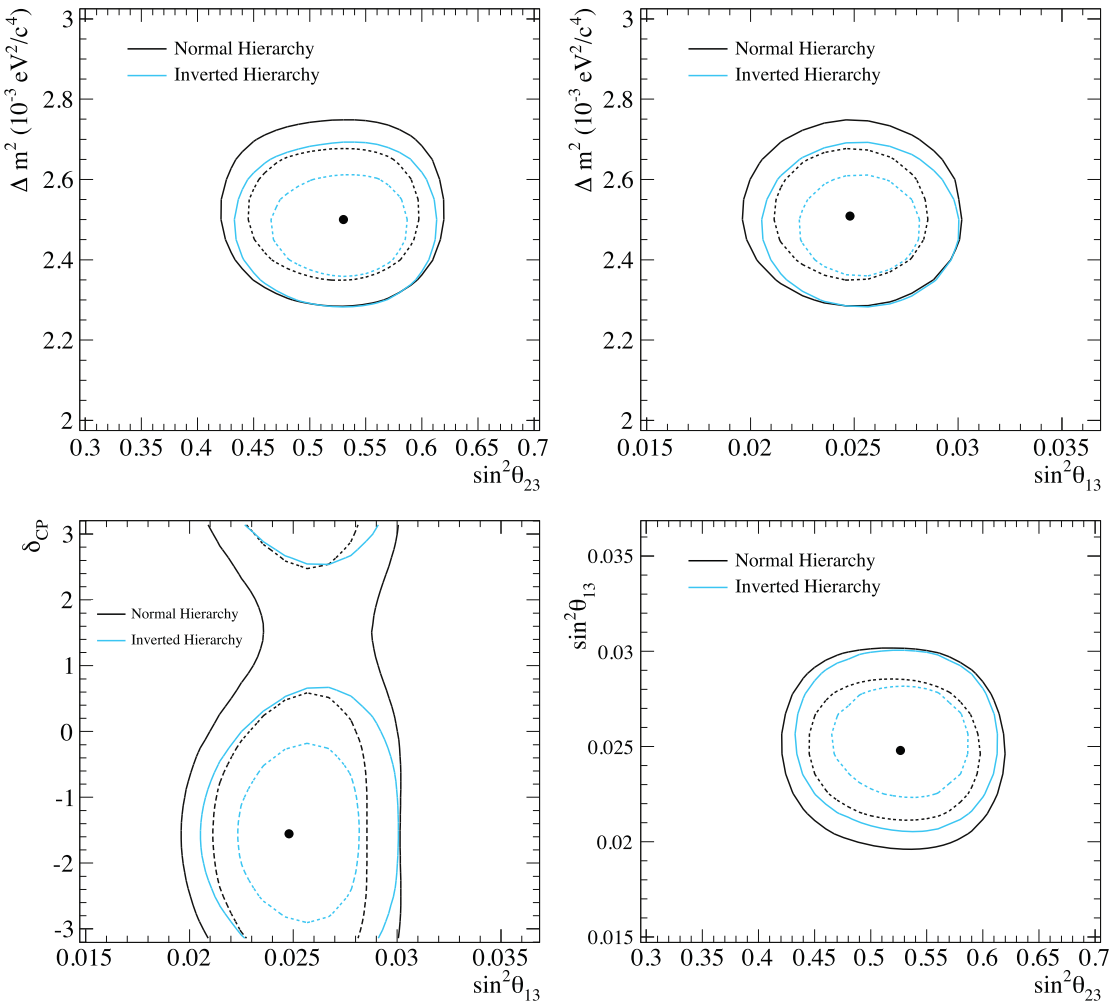

Figure 17. T2K Contours of oscillation parameters calculated with the Δ log L method for both normal and inverted hierarchy cases [29]: (top-left) $\sin^2\theta_{23}$ versus $|\Delta m^2_{32(13)}|$, (top-right) $\sin^2\theta_{13}$ versus $|\Delta m^2_{32(13)}|$, (bottom-left) $\sin^2\theta_{13}$ versus δ_{CP}, and (bottom-right) $\sin^2\theta_{23}$ versus $\sin^2\theta_{13}$. The 90% (68%) C.L. are shown in the solid (dashed) lines with the best fit point shown by the mark.

extracted by fitting two data samples of ν_e and ν_μ simultaneously. For this purpose, the T2K collaboration developed analysis techniques to fit both ν_e and ν_μ samples. One method is based on the Δ log L method, and the other is based on the Markov chain Monte Carlo (MCMC) method. The θ_{13} constraint from PDG2012 [10] is applied in the analysis.

With the Δ log L method, T2K measures $\sin^2 2\theta_{13}$, $\sin^2\theta_{23}$, $\Delta m^2_{32(13)}$ and δ_{CP} as shown in figure 17. The results are consistent with those shown in sections 3.2 and 4.1, and the correlations between parameters are properly treated. With the MCMC method, the quantities $-2\Delta \ln L\,(\equiv \ln L\,(\delta_{CP}) - \ln L\,(\text{best fit values}))$ in the fit, as a function of δ_{CP}, are evaluated as shown in figure 18. The best fit value and the preferred regions at 90% C.L. are consistent with the result of the ν_e only sample shown in figure 13.

In figure 19, the credible intervals calculated in the MCMC method are shown in the $\sin^2\theta_{23}$ versus $|\Delta m^2_{32}|$ plane, for both normal and inverted mass hierarchy cases. The results are compared with other measurements by Super-Kamiokande [27] and MINOS [6]. The T2K best fit point is found to lie in the normal mass hierarchy as shown in figure 19.

5. Systematic uncertainties

5.1. T2K Beam

In accelerator neutrino beam experiments, understanding of the properties of the neutrino beam is very important. An experiment is usually designed to cancel first-order uncertainties of the neutrino beam by adopting the 'two detectors' technique, in which one detector, located near the beam production point, is used to monitor the beam and the other, far detector, studies neutrino oscillations. By normalizing the neutrino

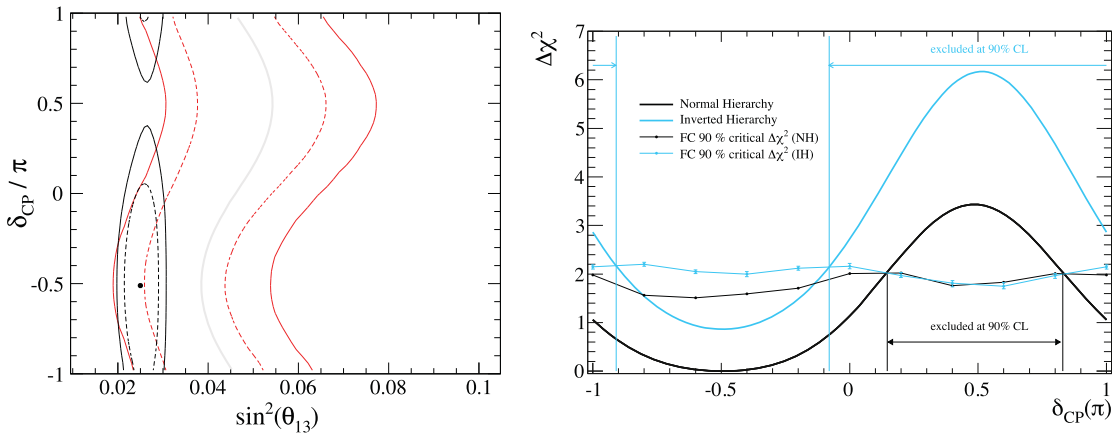

Figure 18. (Left) The T2K credible intervals in the $\sin^2\theta_{13}$ versus δ_{CP} plane calculated in the MCMC method [29]. The 68% intervals are show by the dashed lines and the 90% intervals are by the solid lines. These are constructed by marginalizing over both mass hierarchies. The red lines are extracted only from the T2K data set, and the black line and the point are extracted from both the T2K data set and the reactor θ_{13} constraint. (Right) The $-2\Delta \ln L$ value as a function of δ_{CP} in the MCMC method with both ν_e and ν_μ samples and reactor θ_{13} constraint [29]. The δ_{CP} regions with values above the 90% C.L. lines are excluded.

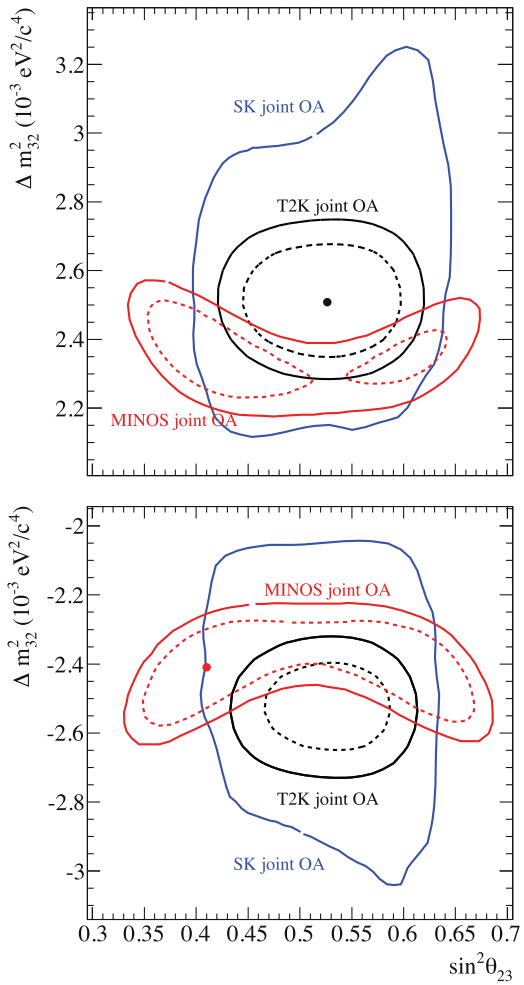

Figure 19. T2K 68% (dashed) and 90% (solid) CL regions contours of oscillation parameters $\sin^2\theta_{23}$ versus Δm^2_{32} for normal (top) and inverted (bottom) mass hierarchy [29]. The best fit point is shown as the black mark in the normal mass hierarchy. The Super-Kamiokande [27] and MINOS [6] results are also shown for comparison.

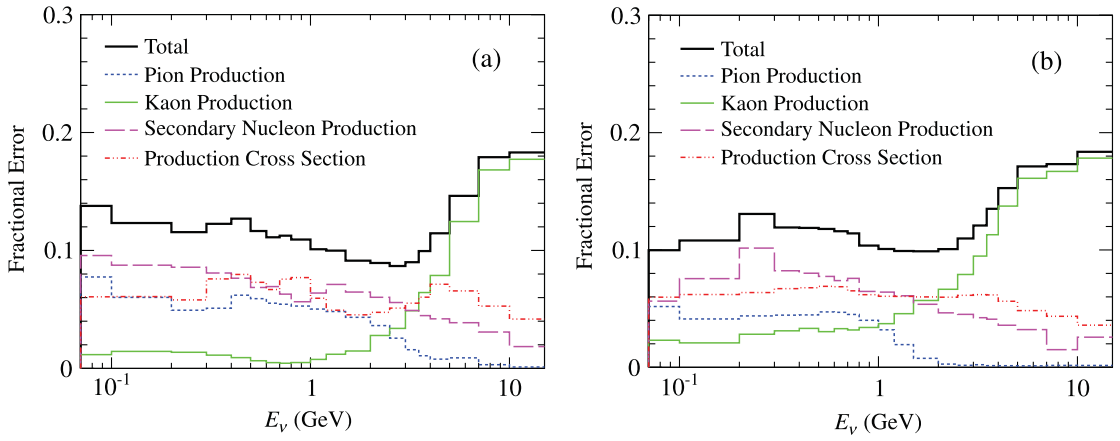

Figure 20. Fractional uncertainty of the T2K neutrino beam flux: (left) muon neutrino component and (right) electron neutrino component [25].

events with the near detector measurement, the systematic uncertainties of the beam and the neutrino cross sections are largely canceled. Even with the cancellation, for a precision measurement, understanding of the beam itself is essential.

In the T2K experiment, the neutrino beam is simulated by incorporating real measurements of hadron production, among which large contributions come from the CERN NA61 experiment [30, 31]. The uncertainties of hadron production decaying into neutrinos are directly related to the systematic uncertainty in the neutrino beam. The uncertainty of the neutrino beam flux at the far detector in the T2K experiment is shown in figure 20.

The fractional uncertainty of the beam is at the 10 $\sim$ 15 % level, of which the largest component is still the uncertainty in hadronic interactions. The second largest component is due to the combined uncertainties of proton beam parameters, alignment of the beam line components and off-axis angle. In T2K, the beam stability and the off-axis angle are directly monitored using the neutrino beam monitor: INGRID [32]. As shown in section 5.2, the relative beam flux uncertainty between the near and far detectors can be reduced to the 3% level including the uncertainty in cross sections constrained by the near detector.

5.2. Constraints by the T2K near detector measurements

The uncertainty of neutrino cross sections is not small, especially in the $\sim$GeV energy region. Although the uncertainty is typically at the $\sim$20% level, the first order uncertainties of the beam and cross sections can be canceled by adopting the two detector technique, as described in section 5.1. For this purpose, MINOS, MINOS+, NOvA and T2K have sophisticated near detectors which collect large amounts of neutrino data to measure the neutrino beam flux and neutrino cross sections with high precision.

In the T2K experiment, the near detector called ND280 [21] is located at 280 m from the beam production target, in the same direction as the far detector, at 2.5° off-axis. ND280 consists of two fine grained detectors, three time projection chambers (TPC), an electromagnetic calorimeter system (ECAL), side muon range detectors (SMRD) and a π^0 detector (P0D). Except for the SMRD, the detectors are located inside a dipole magnet of 0.2 T magnetic field. For neutrino energies around 1 GeV, the dominant neutrino interaction is CC QE scattering, and the second dominant one is CC 1 π production. In the higher energy region, deep-inelastic scattering (DIS) becomes dominant. In ND280, the following three event categories have been measured: CC0π, CC1π and CC Other where the CC0π sample is for CC QE events, CC1π for CC 1 π production and CC Other for DIS. The distributions of muon momentum and scattering angle relative to the neutrino beam are shown in figure 21 for data.

The neutrino interaction models and the neutrino beam flux are tuned to match the observed distributions in figure 21. After tuning, the uncertainties of the neutrino event rates are summarized in table 2. The uncertainties of π hadronic interactions in the far detector and the detector systematic error in the far detector are also shown.

In T2K, the number of observed ν_e (ν_μ) events is 28 (120) with a systematic uncertainty of 6.8 (7.7)%. In figure 22, the uncertainties on the expected energy distributions of both ν_e and ν_μ events are shown before and after constraint by the ND280 measurement. Today, the T2K sensitivity is not very limited by systematic errors

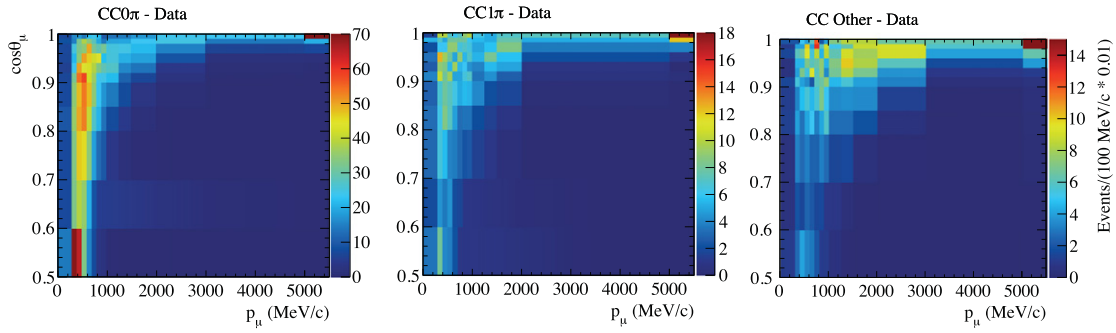

Figure 21. The muon momentum versus the scattering angle for CC0π (left), CC1π (middle) and CC Other (right) samples in T2K data.

Table 2. Fractional uncertainties (%) of the number of neutrino events in the T2K far detector [29]. The uncertainties of cross sections are categorized into two parts: One is constrained by the ND280 measurement, and the other is independent of ND280.

Sources	ν_e candidates	ν_μ candidates
Flux + cross sections (ND280 constrained)	3.2	2.7
Cross sections (ND280 independent)	4.7	5.0
π interactions in the far detector	2.5	3.0
Far detector systematic	2.7	4.0
Total	6.8	7.7

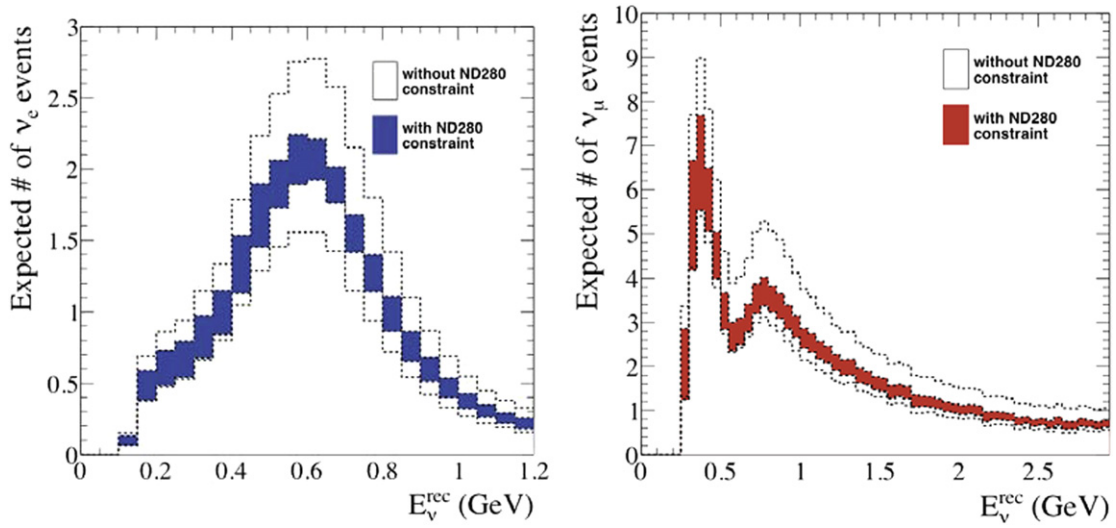

Figure 22. The uncertainty of the neutrino events in the T2K far detector as a function of neutrino energy [29]. (Left) ν_e candidate events and (right) ν_μ candidate events.

which will also rapidly improve for the future CP violation measurement. In the near future, T2K expects that the total systematic uncertainty can be reduced down to 5% or less.

5.3. MINOS systematics

MINOS measurements have significant statistical error. For example, in the combined beam and atmospheric analysis a total of 3117 beam-generated contained-vertex CC events, distributed across the entire neutrino

energy spectrum, are used [33]. The appearance analysis finds 172 events. Notwithstanding these small samples, MINOS has performed complete and detailed analysis of the systematics of the parameter measurements. The sensitivity of the results to systematics also benefits from the great similarity between the MINOS near and far detectors. Here we summarize the most important beam-related systematics and their effects.

The MINOS three-neutrino combined ν_μ disappearance and ν_e appearance paper [6] describes the use of 32 systematic effects as nuisance parameters in the final fits. Of these 13 concern the atmospheric neutrinos; these are not discussed further in this section. There are four dominant systematic effects in ν_μ disappearance in MINOS. These are, with representative values (from [34]):

(1) Hadronic shower energy (7% in the oscillation maximum region),

(2) μ energy (2%–3%, depending on technique),

(3) relative normailzation (1.6%), and

(4) residual NC contamination (20%).

The systematic knowledge of the muon energy includes measurements by range (in the MINOS steel, 2%), and by momentum extracted from curvature in the MINOS magnetic field (3%). The relative normalization error of 1.6% is derived from knowledge of fiducial masses and relative reconstruction efficiencies [34].

Additional systematics are taken into account for ν_e appearance, affecting both signal and background predictions which are compared with the observed data. Many of the large number of systematic checks have small or negligible effects on the measured parameters; nevertheless they are incorporated in the final fitting procedures as discussed above.

Illustrative values of the systematic effects are quoted in [5], where the effect of the relevant uncertainties on the far detector background prediction for ν_e appearance in the ν_μ beam are given as:

(1) Energy scale: this includes both relative energy scale differences between the near and far detectors and the absolute energy scale. The former affects the ν_e background prediction by directly impacting the extrapolation from data, and is the most important single systematic (2%). The latter enters via its effects on the event selection process, and is less important. The combined effect on the background is 2.7%.

(2) Normalization: this term refers to effects relating to the relative fiducial masses and exposures of the two detectors. It is quoted as 1.9%.

(3) ν_τ cross section: a poorly known pseudo-scalar form factor [35] causes a background uncertainty of 1.7%.

(4) All others: small effects due to, for example, neutrino fluxes and cross-sections (which largely cancel due to the functional identity of the near and far detectors) and hadronic shower modeling in neutrino interactions. [36]. The sum of these small effects is $< 1\%$, showing once more the effectiveness of extrapolating from near detector data.

The final uncertainty on the ν_e background is 4%, to be compared with its statistical uncertainty of 8.8%. The numbers cited here apply to the ν_μ beam mode only, with similar, but slightly higher values for the $\bar{\nu}_\mu$ beam mode. In addition, there is a systematic error of approximately 5% on the appearance signal selection efficiency, studied with CC events in which the muon data has been replaced with a simulated electron.

6. Additional measurements

6.1. Additional measurements in MINOS

In addition to the primary mission of MINOS and MINOS+, which is the understanding of the three-neutrino oscillation sector, the MINOS detectors and NuMI beam line are capable of a wide variety of additional measurements which enrich our understanding of the physics of neutrinos, and other areas. Measurements published by the MINOS collaboration include:

(1) Searches for additional sterile neutrinos using charged and NC interactions [37, 38],

(2) measurement of neutrino cross-sections [39],

(3) tests of fundamental symmetries and searches for non-standard interactions [40],

(4) studies of cosmic rays at both near and far detectors [41].

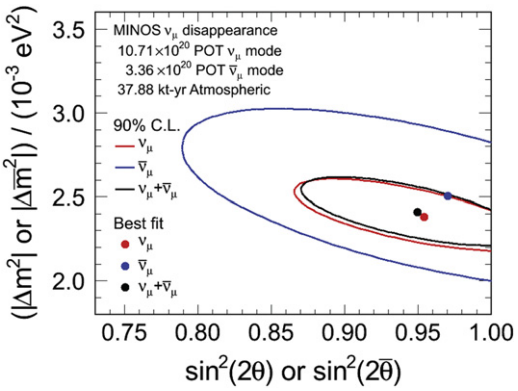

Figure 23. MINOS comparison of ν_μ and $\bar{\nu_\mu}$ oscillations from [33]. The 90% confidence level allowed regions and best fit values are shown for ν_μ and $\bar{\nu_\mu}$ oscillations, and for a fit in which the parameters are assumed to be identical.

Table 3. Neutrino cross sections measurements in T2K for charged–current (CC) and neutral current (NC) inclusive processes. The measurements of cross sections are given per nucleon. The ratio of cross sections is also shown in some measurements.

Mode	Results ($\frac{\text{cm}^2}{\text{nucleon}}$ or the ratio)	$\langle E_\nu \rangle$ (GeV)	Reference
ν_μ CC inclusive	$(6.91 \pm 0.13\,(\text{stat}) \pm 0.84\,(\text{syst})) \times 10^{-39}$	0.85	[42]
ν_e CC inclusive	$(1.11 \pm 0.09\,(\text{stat}) \pm 0.18\,(\text{syst})) \times 10^{-38}$	∼1.3	[43]
ν_μ CC inclusive on Fe	$(1.444 \pm 0.002\,(\text{stat})^{+0.189}_{-0.157}\,(\text{syst})) \times 10^{-38}$	1.51	[44]
ν_μ CC inclusive on CH	$(1.379 \pm 0.009\,(\text{stat})^{+0.178}_{-0.147}\,(\text{syst})) \times 10^{-38}$	1.51	[44]
ν_μ CC ratio of Fe/CH	$1.047 \pm 0.007\,(\text{stat}) \pm 0.035\,(\text{syst})$	1.51	[44]
ν_μ CC-QE on CH	$(10.64 \pm 0.37\,(\text{stat})^{+2.03}_{-1.65}\,(\text{syst})) \times 10^{-39}$	0.93	[45]
ν_μ CC-QE on CH	$(11.95 \pm 0.19\,(\text{stat})^{+1.82}_{-1.47}\,(\text{syst})) \times 10^{-39}$	1.94	[45]
NC γ	$(1.55^{+0.65}_{-0.33}) \times 10^{-38}$	0.63	[46]
ν_e CC ratio	$\sigma_{\nu_e CC}/\sigma_{\text{prediction}} = 1.01 \pm 0.10$	∼1.3	[47]
ν_e (K decay) CC ratio	$\sigma_{\nu_e CC}/\sigma_{\text{prediction}} = 0.68 \pm 0.30$	—	[47]
ν_e (μ decay) CC ratio	$\sigma_{\nu_e CC}/\sigma_{\text{prediction}} = 1.10 \pm 0.14$	—	[47]

In this section we discuss briefly the first item, searches for sterile neutrinos, and present an example of a fundamental symmetry test.

Anomalies seen in short baseline experiments [48] and others have generated great interest in the possibility of a fourth neutrino which would not have standard model interactions. NCs in the MINOS detectors are visible as hadronic showers without an accompanying lepton. All active flavors of neutrinos produce NCs equivalently, so that the three-neutrino oscillation phenomenon should not cause any depletion with respect to expectations in the observed far detector spectrum. This is indeed seen to be the case, as documented in [38] which measures a limit on the fraction of neutrinos which can have oscillated to sterile neutrinos, f_s, of $f_s < 22\%$. More recently, preliminary analysis of further data has generated limits on the sterile mixing angle θ_{24} which extend the range of previous experiments [49].

A fundamental test of CPT symmetry is the equivalence of oscillation parameters obtained from ν_μ and $\bar{\nu_\mu}$. The magnetized MINOS detector can perform an event-by-event comparison of these parameters enabling an accurate test of this prediction. The resulting allowed regions (from [33]) are displayed in figure 23. The difference in $|\Delta m^2|$ obtained, in a two-flavor model, is $|\Delta\bar{m}^2| - |\Delta m^2| = (0.12^{+0.24}_{-0.26}) \times 10^{-3}$ eV^2.

6.2. Additional measurements in T2K

In addition to neutrino oscillation studies, T2K conducts various measurements on neutrino-nucleus cross sections. As described in section 5.2, the understanding of neutrino cross sections is important to reduce systematic uncertainties of neutrino oscillation measurements, which could improve the sensitivity to neutrino oscillations.

The cross sections measured in T2K are summarized in table 3. As the first step, T2K measures the muon neutrino CC inclusive cross sections with the T2K off-axis near detector (ND280) [42] and the on-axis near detector (INGRID) [44]. In future, these analyzes will be more sophisticated to measure exclusive channels, such as CC-QE, CC 1π production, and CC-coherent π, as energy dependent differential cross sections. With INGRID, there are two types of neutrino detector with different target materials. One has an iron target, and the

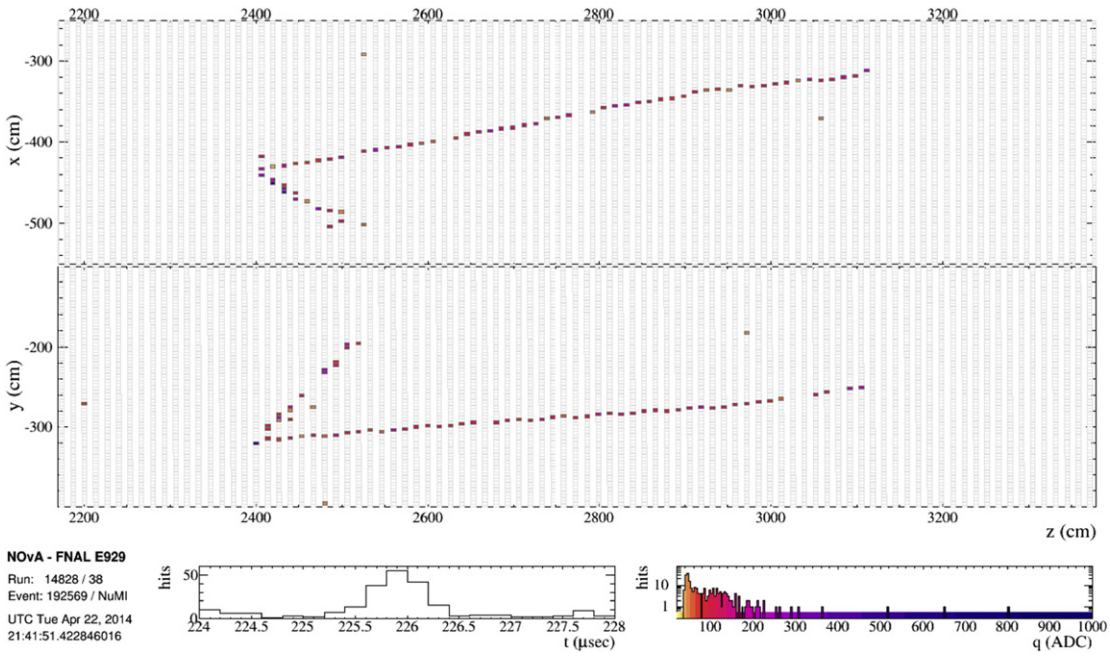

Figure 24. Charged–current neutrino interaction observed in the NOvA Far Detector (Courtesy NOvA Collaboration).

other has a plastic (CH) target. By using two targets, the CC inclusive cross sections on iron and plastic, and the ratio of cross sections are measured. The CC-QE cross sections are also measured with the CH target [45]. With ND280, the electron neutrino CC inclusive cross sections can also be measured [43, 47], using the powerful particle identification performance of TPC and ECAL. In the analysis [47], the electron neutrino contamination in the beam is measured relative to the prediction in the simulation. T2K also has divided the measurement into two contributions: One is the electron neutrino from kaon decay and the other is from muon decay. The NC gamma production cross section in neutrino-oxygen interaction has also been measured [47] by using the far detector, Super-Kamiokande. All the results are consistent with the predictions in the neutrino interaction generator libraries NEUT [50] and GENIE [51]. Finally, with ND280, the electron neutrino disappearance sample was searched to investigate neutrino oscillations to sterile neutrinos [52].

7. The frontier and future sensitivity

7.1. NOvA

The NOvA experiment is the principal appearance-mode long-baseline experiment at Fermilab. It makes use of the off-axis NuMI beam as discussed in previous sections. The far and near detectors minimize passive mass, moving toward the ideal of a totally active fiducial volume which will be realized with future detectors, such as e.g. DUNE liquid argon TPC's. A totally active detector typically has better performance because all charged particles in neutrino interactions are reconstructed properly with good efficiency. In the case of NOvA the active medium is liquid scintillator mixed into oil. The basic segmentation of the detector is planes of 3.6 cm $\times$ 5.6 cm PVC tubes, separated by thin walls. Light is collected in each tube by a looped wavelength shifting fiber that is directed onto a single pixel of an avalanche photodiode (APD). The APD's are cooled by a hybrid thermoelectric/water system to a temperature of -15° C.

There are a total of 344 064 tubes arranged in an interchanging pattern of horizontal and vertical planes, giving an active structure 15.6 m $\times$ 15.6 m, and 60 m long. The active scintillator mass is 8.7 ktonnes with 5.3 ktonnes devoted to the PVC support structure, fiber readout, and other structural components, giving a total far detector mass of 14.0 ktonnes. Figure 24 shows a typical NOvA far detector event.

In addition to the far detector, a functionally equivalent near detector is located at Fermilab. This detector consists of horizontal planes 4.0 m $\times$ 4.0 m, together with a steel muon catcher to assist in measurement of the spectrum of CC events. The expected average occupancy of the near detector is $\approx$6 events per spill at full intensity, which will be separated by their time of occurrence, as is already successfully done in MINOS and MINERvA.

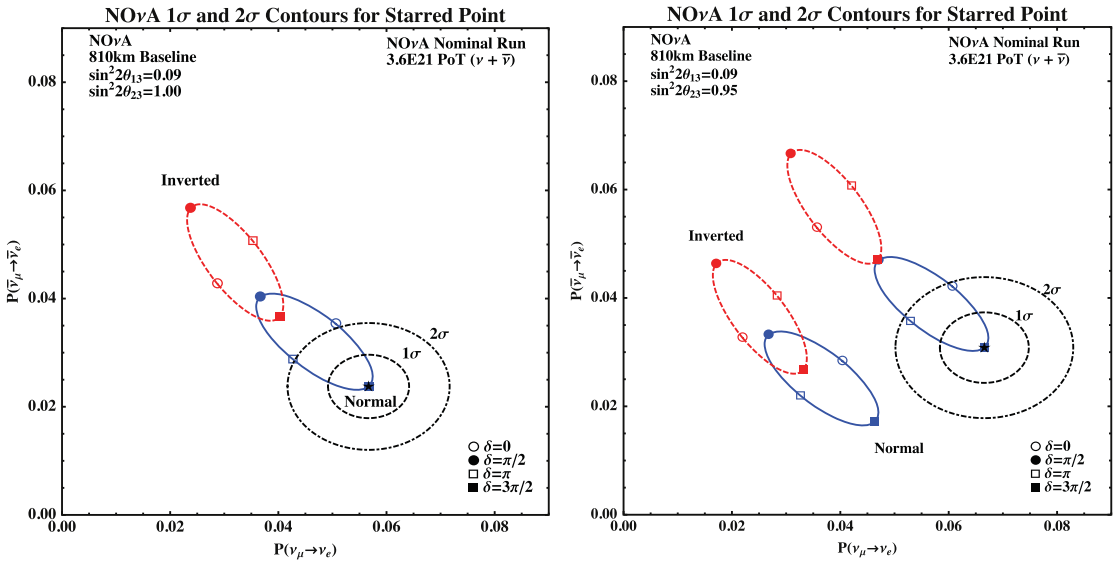

Figure 25. Biprobability plot showing the effect of mass hierarchy, δ_{CP}, and ν_μ versus $\bar{\nu}_\mu$ exposure. The left panel shows the expected appearance probabilities for ν_e ($\bar{\nu}_e$) when the mixing angle $\theta_{23} = \pi/4$ (maximal mixing). The right panel shows the same for assumed non-maximal mixing with $\theta_{23} < \pi/4$ and $\theta_{23} > \pi/4$. (Courtesy NOvA Collaboration.)

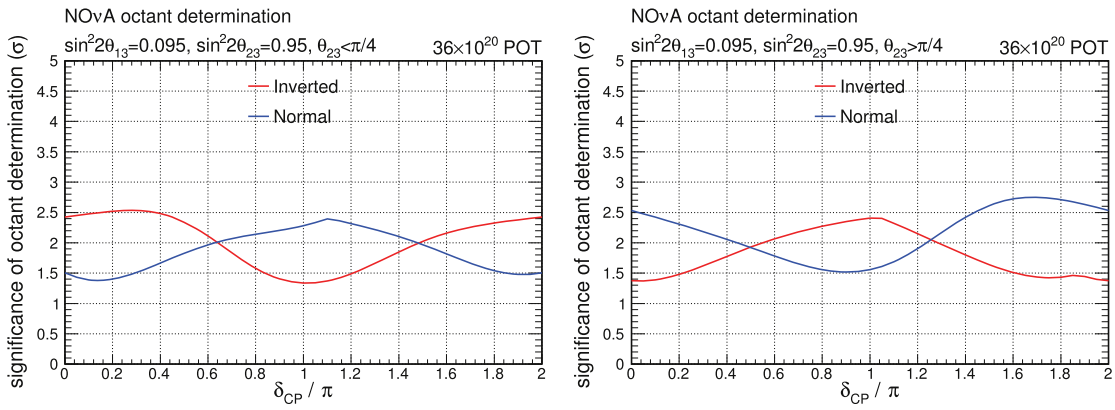

Figure 26. NOvA sensitivities for resolution of the octant of non-maximal θ_{23}, assumed to be at $\sin^2 2\theta_{23} = 0.95$. Left (right) panel shows the sensitivity for $\theta_{23} < \pi/4$ ($\theta_{23} > \pi/4$). (Courtesy NOvA Collaboration.)

The relatively large value of θ_{13} provides the opportunity for a rich harvest of physics results for NOvA via both disappearance and appearance, with both neutrino and antineutrino beams. Here we focus on the appearance channel, with its rich information about θ_{13}, mass hierarchy, and δ_{CP}. Disappearance measurements are also highly sensitive and give excellent information on the octant of θ_{23}. During early running, combination with MINOS+ will be exploited, as discussed separately below.

As discussed in earlier sections, the measurements of ν_e appearance of NOvA are significantly affected by matter effects, potential CP violation, mass hierarchy, and the distinctions between neutrinos and anti-neutrinos. A useful tool for understanding these dependencies is the biprobability plot, in which one axis displays the appearance probability for ν_e and the other the probability for $\bar{\nu}_e$. Figure 25 shows this situation graphically, for the case of maximal mixing. The results are clearly separated for many values of δ_{CP}, with areas of overlap for the regions around $\delta_{CP} = \pi/2$ ($\delta_{CP} = 3\pi/2$) for normal (inverted) mass hierarchy. Moreover, the subleading effects cause a separation in the appearance probabilities depending on the octant of θ_{23}.

The sensitivity of NOvA to the octant depends on the value of θ_{23}, and somewhat on both the hierarchy and the value of δ_{CP}. For a value of $\sin^2 2\theta_{23}$ of 0.95, there is considerable sensitivity for all values of those parameters, exceeding 95% CL for significant portions of the parameter space with the nominal exposure, shown in figure 26.

As suggested by figure 25, a principle goal of NOvA is to gain information about the mass hierarchy of the neutrino eigenstates. We can see the sensitivity of a 'standard' expected exposure in the NuMI beam in figure 27.

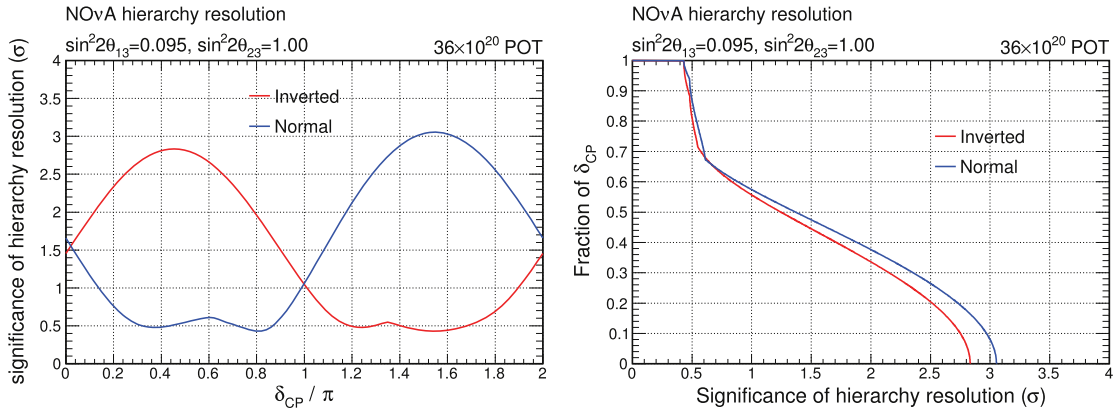

Figure 27. Sensitivity of NOvA to the neutrino mass hierarchy. The left panel shows the sensitivity as a function of δ_{CP}/π. The right panel shows the fraction of δ_{CP} space covered for various degrees of statistical significance σ. Both plots are for maximal θ_{23}. Approximate one third of the δ_{CP} range gives a hierarchy determination at 95% C.L. (Courtesy NOvA Collaboration).

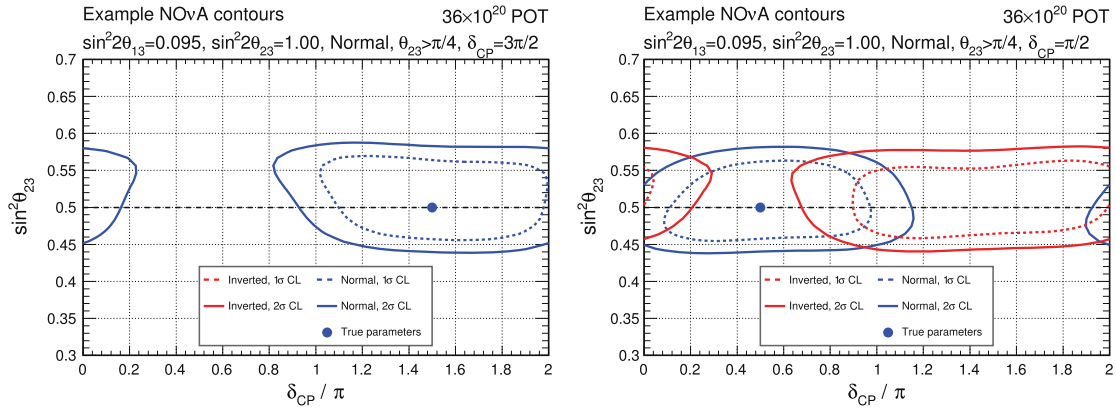

Figure 28. Examples of joint NOvA sensitivity contours for $\sin^2\theta_{23}$ and δ_{CP}, for a nominal run of 36×10^{20} protons on target in the 700 kW NuMI beam. In the left panel θ_{23} is maximal, and δ_{CP} is chosen for maximum separation between the hierarchies. The inverted hierarchy and some values of δ_{CP} are disfavored. A less-favorable case is shown in the right panel, where δ_{CP} is chosen to illustrate the difficulty of distinguishing the hierarchies. In both-cases θ_{13} is taken as an external input (Courtesy NOvA Collaboration).

Hierachy and CP violation information are coupled, leading to the right panel of the figure, in which the fractional coverage of 'CP-space' $0 - 2\pi$ at which the hierarchies can be separated is shown as a function of the significance of the separation.

Because of parameter ambiguities, the study of CP violation in neutrino oscillations is particularly challenging. Full resolution of the problem may require the very large detectors of Hyper-K and DUNE, currently under discussion. However, particularly in favorable cases, important information can be obtained. Figure 28 illustrates the situation by plotting the simultaneous significance of two quantities, $\sin^2\theta_{23}$ and δ_{CP}, for both hierarchies. In confused cases information is obtained about the likely correlations of δ_{CP} and the hierarchy, and less ambiguous cases will favor specific regions of δ_{CP}.

7.2. MINOS+

The MINOS experiment, as described in this paper, has studied the region in L/E near the oscillation minimum in detail, using primarily low-energy settings of the NuMI beam. As discussed in section 2.2 the requirements of off-axis kinematics for the NOvA experiment lead to a need for a higher energy on-axis setting of the on-axis beam. This beam, with its associated larger event rates in both MINOS near and far detectors, is exploited by the MINOS+ experiment. Figure 29 shows the expected structure of the data spectrum which will be obtained by MINOS+. The experiment, will collect on the order of 3000 CC and 1200 NC events for each exposure of 6.0×10^{20} protons on the NuMI target (roughly annually). These large event rates allow a varied physics program.

Representative physics goals of the MINOS+ experiment include:

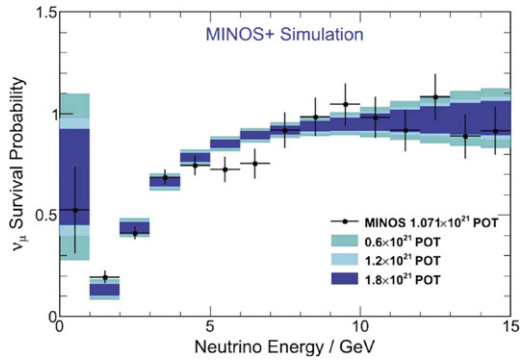

Figure 29. Ratio of oscillated to unoscillated predictions for ν_μ charged–current events in the MINOS+ experiment, as a function of exposure in terms of protons on target (POT). The statistical precision in the neutrino energy region of 5–7 GeV is much improved by the high rates available from the NuMI complex (Courtesy MINOS+ Collaboration).

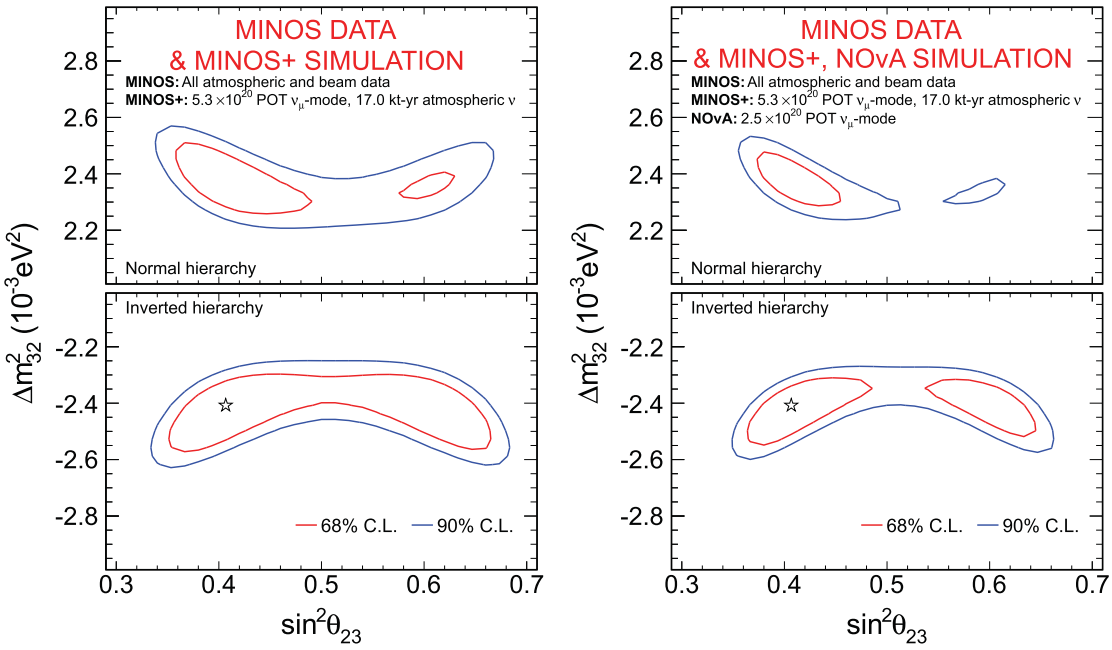

Figure 30. Expected near-term precision of determination of the oscillation parameters $\sin^2\theta_{23}$ and Δm^2_{32} for the MINOS+ experiment. The left panel shows the results when MINOS and MINOS+ data are combined, and the right panel includes the expected data from the NOvA experiment. The contours are generated using as inputs the best-fit MINOS values from [6] (Courtesy MINOS+ Collaboration).

(1) Precise verification of the expected spectral shape of the oscillation phenomenon, using the disappearance technique, especially in its transition region in energy between 5 and 7 GeV.

(2) Utilization of the precise spectrum together with MINOS and NOvA data to continue improving understanding of the oscillation parameters.

(3) Further study of the possibilities of sterile neutrinos, using both CC and NC disappearance.

(4) Improved precision on searches for exotic phenomena.

Figure 30 shows an example of (ii), considering all the NuMI program data expected to be obtained in the 2015 time frame. Comparison with figure 16 shows improved determination of the parameters, especially in the case of the normal mass hierarchy.

Table 4. The expected number of ν_e events in T2K with 7.8×10^{21} POT for the neutrino beam mode and 7.8×10^{21} POT for the ant-neutrino [53].

Beam Mode	Total	Signal $\nu_\mu \to \nu_e$	Signal $\overline{\nu}_\mu \to \overline{\nu}_e$	Beam CC $\nu_e + \overline{\nu}_e$	Beam CC $\nu_\mu + \overline{\nu}_\mu$	NC NC
Neutrino beam	291.5	211.9	2.4	41.3	1.4	34.5
Anti-neutrino beam	94.9	11.2	48.8	17.2	0.4	17.3

Table 5. The expected number of ν_μ events in T2K with 7.8×10^{21} POT for each beam operation mode [53].

Beam Mode	Total	CCQE $\nu_\mu(\overline{\nu}_\mu)$	CC non-QE $\nu_\mu(\overline{\nu}_\mu)$	CC $\nu_e + \overline{\nu}_e$ $\nu_\mu(\overline{\nu}_\mu) \to \nu_e(\overline{\nu}_e)$	NC
Neutrino beam	1493	782 (48)	544 (40)	4	75
Anti-neutrino beam	715	130 (263)	151 (138)	0.5	33

7.3. Future prospects of T2K

The approved beam for the T2K experiment is 7.8×10^{21} POT. The results of T2K reported in this paper are based on 6.6×10^{20} which is only 8% of the original goal[7]. In the near future, the J-PARC accelerator plans to increase the repetition rate of the acceleration cycle by updating the power supply system. With the upgrade, the beam power of J-PARC will reach 750 kW, and T2K will accumulate the design beam within several years. In this section, we show the physics sensitivity of T2K with 7.8×10^{21} POT. In T2K, there are two beam operation modes: one is neutrino beam and the other is anti-neutrino beam. Since the fraction of the anti-neutrino beam to the neutrino is not fixed yet, we will show both possibilities.

The current goals of T2K with 7.8×10^{21} POT are

- Initial measurement of CP violation in neutrinos up to a 2.5 σ level of significance.
- Precision measurement of oscillation parameters in the ν_μ disappearance with precision of $\delta\Delta m^2_{32} \simeq 10^{-4}$ eV^2 and $\delta \sin^2 2\theta_{23} \simeq 0.01$; also determination of θ_{23} octant at 90% C.L. if $|\theta_{23} - 45°| > 4°$.
- Contribution to the determination of the mass hierarchy.

7.3.1. Neutrino events with 7.8×10^{21} protons on target (POT)

Based on the analysis method in [25, 26], the expected number of ν_e and ν_μ events[8] are shown in tables 4 and 5 using the following neutrino oscillation parameters: $\sin^2 2\theta_{13} = 0.1$, $\sin^2 \theta_{23} = 0.5$, $\sin^2 2\theta_{12} = 0.8704$, $\Delta m^2_{12} = 7.6 \times 10^{-5}$ eV^2, $|\Delta m^2_{32}| = 2.4 \times 10^{-3}$ eV^2, $\delta_{CP} = 0$, and $\Delta m^2_{32} > 0$.

7.3.2. CP sensitivity

Since the electron neutrino appearance is sensitive to CP violation, the variation of the number of electron neutrino events with δ_{CP} parameters is shown in figure 31. In maximum, we expect a 27% change, compared to no CP violation with $\delta_{CP} = 0$. Hereafter, we assume the beam exposure to be 50% for the neutrino beam and 50% for the anti-neutrino. We also assume $\sin^2 2\theta_{13} = 0.10 \pm 0.005$ as the ultimate θ_{13} value from reactor experiments. In the case of the maximum CP violation ($\delta_{CP} = -90°$), the T2K sensitivity for $\delta_{CP} = -90°$ is shown in figure 32 with 90% C.L.

In reality, the sensitivity to CP violation also depends on θ_{23}. In figure 33, as the T2K sensititivy, we show the χ^2 difference between the true point with (δ_{CP}, $\sin^2 \theta_{23}$) and the hypothesis test point with $\delta_{CP} = 0$.

7.3.3. Precision measurements of neutrino oscillation parameters

Since most of the T2K measurements are limited by statistics, more data improve the precision of the measurements. Among the oscillation parameters, $\sin^2\theta_{23}$ and $|\Delta m^2_{32}|$ are interesting because of their relatively larger uncertainty compared to other parameters. Figure 34 shows the expected precision of $\sin^2 \theta_{23}$ and $|\Delta m^2_{32}|$ as a function of POT for the normal mass hierarchy case. Hereafter, the total exposure in T2K is assumed to be

[7] T2K collected 1.0×10^{21} POT on March 26th, 2015.

[8] This study was conducted before T2K developed the special π^0 rejection algorithm. So, the number of NC background is higher, compared to the results in section 3.2.

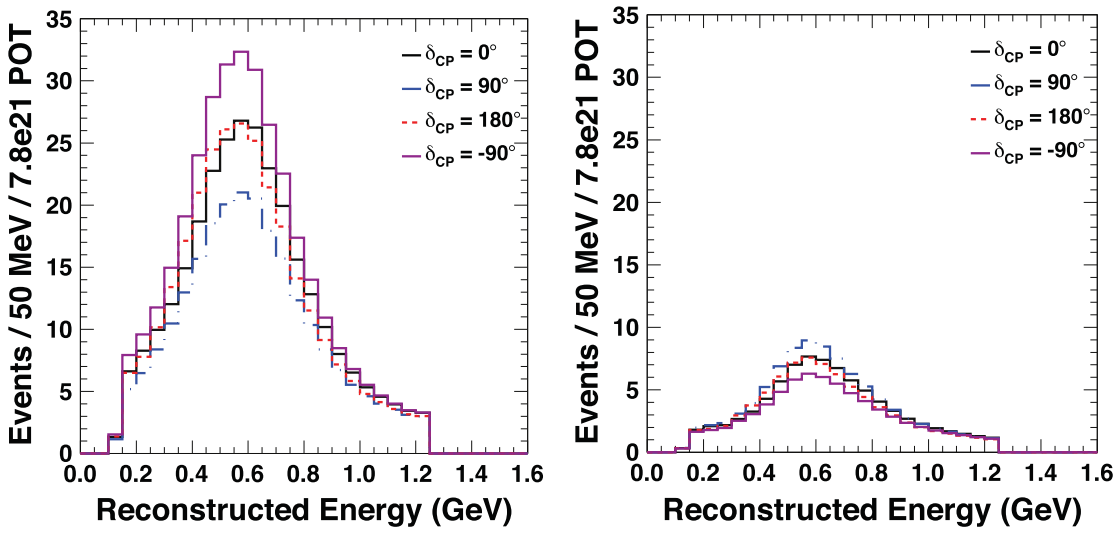

Figure 31. The reconstruction energy of expected T2K electron neutrino appearance events with various δ_{CP} parameters [53]. (Left) Neutrino beam operation with 7.8 $\times$ 10^{21} POT and (right) anti-neutrino beam operation with 7.8 $\times$ 10^{21} POT.

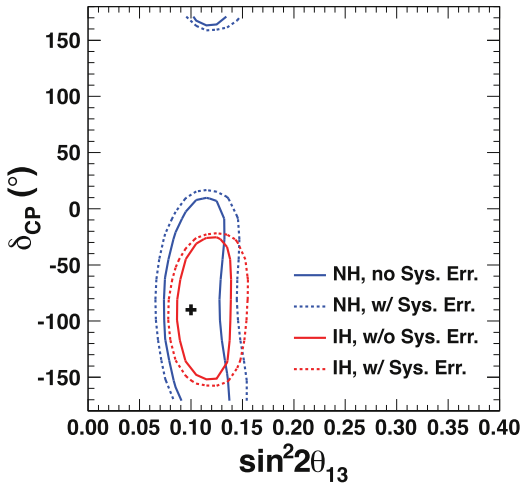

Figure 32. The 90% contour region of the δ_{CP} versus $\sin^2 2\theta_{13}$ plane in the expected T2K sensitivity with 7.8 $\times$ 10^{21} POT [53]. POT are assumed to be equally distributed to the neutrino beam mode (3.9 $\times$ 10^{21} POT) and the anti-neutrino (3.9 $\times$ 10^{21} POT).

7.8 $\times$ 10^{21} POT which are equally distributed to the neutrino beam mode (3.9 $\times$ 10^{21} POT) and the anti-neutrino (3.9 $\times$ 10^{21} POT).

The statistical uncertainty of $\sin^2\theta_{23}$ and $|\Delta m^2_{32}|$ is 0.045 and 0.04 $\times$ 10^{-3} eV^2, respectively, at the T2K full statistics. The precision of $\sin^2\theta_{13}$ is influenced by the precision of other oscillation parameters including $\sin^2\theta_{23}$ and δ_{CP}.

An interesting question about θ_{23} is which θ_{23} is exactly 45° or not. In the case of $\theta_{23} \neq 45°$, which octant does the value of θ_{23} fit in, ($\theta_{23} > 45°$ or $\theta_{23} < 45°$)? Figure 35 shows the region where T2K can reject the maximum mixing $\theta_{23} = 45°$ and the regions where T2K can reject one of the octants of θ_{23}. The octant of θ_{23} is determined at 90% C.L. if $|\theta_{23} - 45°| > 4°$.

7.3.4. Mass hierarchy

Because of the relatively short baseline (~300 km) of T2K, the experiment is less sensitive to the mass hierarchy (more sensitive to CP). However, the measurement of T2K (sensitive to CP) can contribute to improving the mass hierarchy sensitivity of NOvA by helping untangle the two effects of CP and mass hierarchy in NOvA. Figure 36 shows the 90% sensitivity region for mass hierarchy with the T2K and NOvA measurements. The

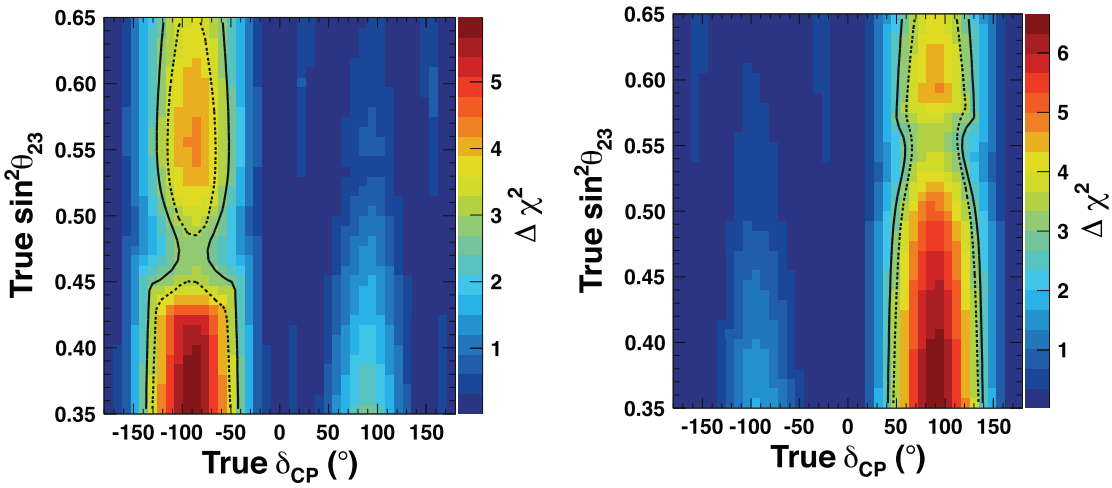

Figure 33. T2K expected χ^2 difference between the true point (δ_{CP}, $\sin^2\theta_{23}$) and the point $\delta_{CP} = 0$ [53]. The map of χ^2 difference shown in color is calculated assuming no systematic errors. The solid contours show the 90% C.L. sensitivity with statistical error only, while the dashed contours include the 2012 T2K systematic error. (Left) The contour in the case of normal mass hierarchy, and (right) in the case of Inverted mass hierarchy. POT are assumed to be equally distributed to the neutrino beam mode (3.9×10^{21} POT) and the anti-neutrino (3.9×10^{21} POT).

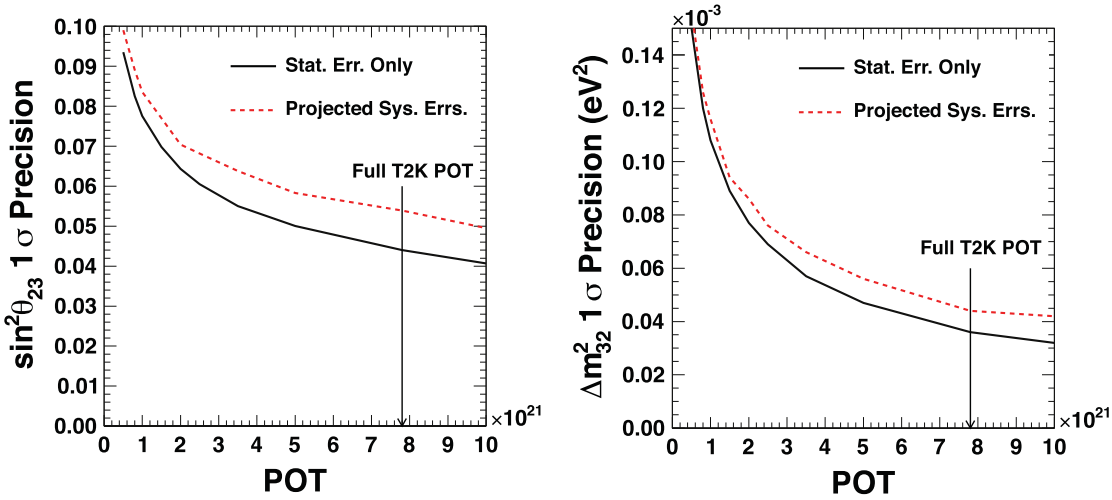

Figure 34. T2K expected sensitivity to $\sin^2\theta_{23}$ and $|\Delta m^2_{32}|$ as a function of POT for the normal mass hierarchy [53]. The solid lines are without systematic error and the dashed one with the systematic error from the T2K 2012 analysis. POT are assumed to be 3.9×10^{21} POT for the neutrino beam mode and 3.9×10^{21} for the anti-neutrino.

sensitivity is really expanded by adding the T2K measurements, especially for $\delta_{CP} \sim 90°(-90°)$ case in the normal (inverted) hierarchy case.

8. Conclusions; building the future

We have presented the results and prospects of neutrino oscillation measurements by the present generation of experiments: MINOS/MINOS+, T2K and NOvA. The phenomenology of neutrinos is being rapidly revealed by these experiments with a dramatical improvement of the precision of neutrino oscillation parameters in 10 years. In the standard neutrino oscillation scenario, all three mixing angles have been measured and found to be large enough to explore CP violation. Surprisingly, the new data from the accelerator experiments is beginning to become sensitive to CP violation, when coupled with the precise knowledge of the mixing angles.

Upcoming results from on-going experiments, especially T2K and NOvA, will have large impact for the following reasons.

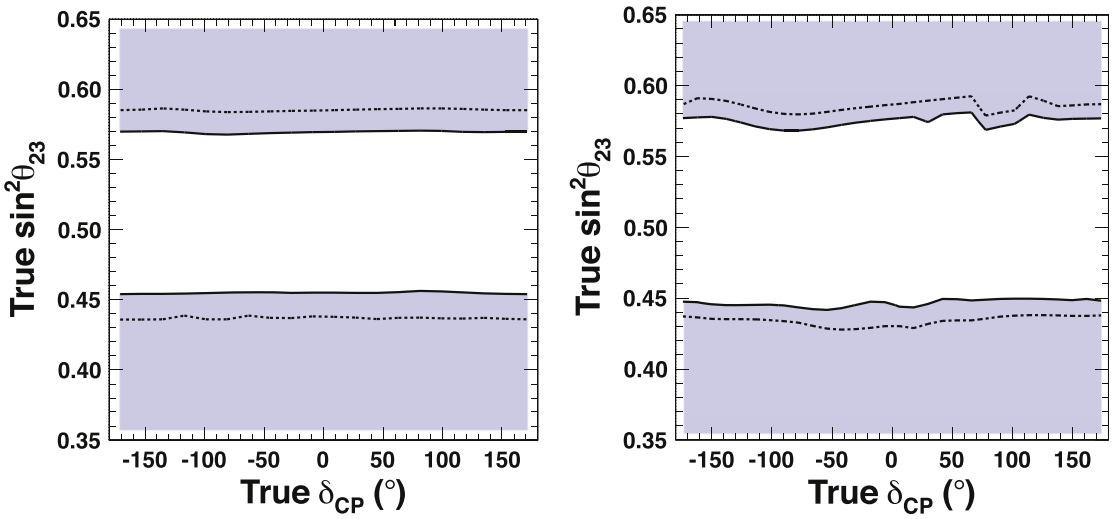

Figure 35. (Left)The shaded region is where T2K has more than a 90% C.L. sensitivity to reject maximal mixing [53]. (Right) The shaded region is where T2K has more than a 90% C.L. sensitivity to reject one of the octants of θ_{23}[53]. The mass hierarchy is considered unknown in the normal mass hierarchy case. The shaded region is calculated assuming no systematic errors (statistical error only), and the dashed contours show the sensitivity including the systematic errors. POT are assumed to be 3.9×10^{21} POT for the neutrino beam mode and 3.9×10^{21} for the anti-neutrino.

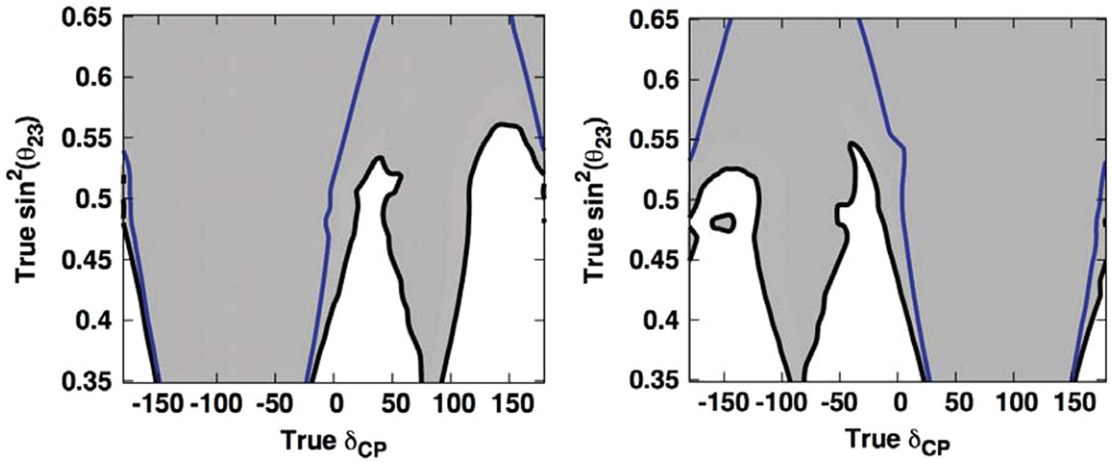

Figure 36. The regions where the wrong mass hierarchy is expected to be rejected at 90% C.L. by the NOvA measurement (blue line) and the NOvA + T2K measurements (black shaded regions) [53]. (Left) The true hierarchy is normal and (right) it is inverted. The T2K POT are assumed to be 3.9×10^{21} POT for the neutrino beam mode and 3.9×10^{21} for the anti-neutrino. The NOvA POT (3.6×10^{21}) are also assumed to be distributed to the neutrino beam mode and the anti-neutrino equally.

- The measurements of T2K and NOvA individually are the most sensitive to CP violation. By combining both, the sensitivity will be further improved.
- In order to explore CP violation, the precision of mixing angles is essential. In particular, the value of θ_{23} plays a key role in specifying the complicated parameter space of delta-CP and the mass hierarchy. These experiments are the most sensitive to θ_{23}.
- The NOvA experiment has some sensitivity to the mass hierarchy. By combining with T2K, the sensitive region will be expanded.
- The future neutrino experiment, Hyper-Kamiokande and DUNE, will have greatly expanded sensitivity to CP violation. The experiences of T2K and NOvA, together with the improvement of systematic uncertainties are key inputs to the future experiments.

Going beyond the standard neutrino oscillation scenario, unexpected phenomena may appear in the most sensitive experiments. Thus, there is discovery potential for MINOS/MINOS+, T2K and NOvA at any time.

Success of on-going experiments is building the future.

Acknowledgments

Fermilab is operated by Fermi Research Alliance, LLC under Contract No. DE-AC02-07CH11359 with the United States Department of Energy. J-PARC is operated by KEK and JAEA with MEXT in Japan. An author (TN) acknowledges the support of MEXT and JSPS in Japan with the Grant-in-Aid for Scientific Research A 24244030 and for Scientific Research on Innovative Areas 25105002 titled 'Unification and Development of the Neutrino Science Frontier'. Fruitful discussions with members of the T2K, MINOS+, and NOvA collaborations are gratefully acknowledged.

References

[1] Ahn M H *et al* (K2K Collaboration) 2006 *Phys. Rev.* D **74** 072003
[2] Abe K *et al* T2K Collaboration 2014 *Phys. Rev. Lett.* **112** 181801
[3] Abe K *et al* (T2K Collaboration) 2014 *Phys. Rev. Lett.* **112** 061802
[4] Agafonova N *et al* (OPERA Collaboration) 2014 *Phys. Rev.* D **89** 051102
[5] Adamson P *et al* 2013 *Phys. Rev. Lett.* **110** 171801
[6] Adamson P *et al* 2014 *Phys. Rev. Lett.* **112** 191801
[7] Fukuda Y *et al* (Super-Kamiokande Collaboration) 1998 *Phys. Rev. Lett.* **81** 1562
[8] Ashie Y *et al* (Super-Kamiokande Collaboration) 2005 *Phys. Rev.* D **71** 112005
[9] Abe K *et al* (Super-Kamiokande Collaboration) 2013 *Phys. Rev. Lett.* **110** 181802
[10] Beringer J *et al* (Particle Data Group Collaboration) 2012 *Phys. Rev.* D **86** 010001
[11] An F P *et al* (Daya Bay Collaboration) 2013 *Chin. Phys.* C **37** 011001
Ahn J K *et al* (RENO Collaboration) 2012 *Phys. Rev. Lett.* **108** 191802
Abe Y *et al* (Double Chooz Collaboration) 2012 *Phys. Rev.* D **86** 052008
[12] Nunokawa H, Parke S and Funchal R Z 2005 *Phys. Rev.* D **72** 013009
[13] Cervera A, Donini A, Gavela M B, Gomez Cadenas J J, Hernandez P, Mena O and Rigolin S 2000 *Nucl. Phys.* B **579** 17
Cervera A, Donini A, Gavela M B, Gomez Cadenas J J, Hernandez P, Mena O and Rigolin S 2001 *Nucl. Phys.* B **593** 731 (erratum)
[14] Freund M 2001 *Phys. Rev.* D **64** 053003
[15] Zwaska R M 2005 *PhD Thesis* FERMILAB-THESIS-2005-73
[16] Adamson P *et al* 2008 *Phys. Rev.* D **77** 072002
[17] Adamson P *et al* 2012 *Phys. Rev. Lett.* **108** 191801
[18] Beavis D *et al* (E889) 1995 Long Baseline Neutrino Oscillation Experiment at the AGS
[19] Abe K *et al* (T2K Collaboration) 2013 *Phys. Rev.* D **87** 012001
[20] NOvA Proposal FNAL-P-0929 arXiv:hep-ex/0503053
[21] Abe K *et al* (T2K Collaboration) 2011 *Nucl. Instrum. Methods* A **659** 106
[22] Adamson P *et al* 2011 *Phys. Rev. Lett.* **107** 181802
[23] Adamson P *et al* 2010 *Phys. Rev.* D **82** 051102(R)
[24] Abe K *et al* (T2K Collaboration) 2011 *Phys. Rev. Lett.* **107** 041801
[25] Abe K *et al* T2K Collaboration 2013 *Phys. Rev.* D **88** 032002
[26] Abe K *et al* (T2K Collaboration) 2013 *Phys. Rev. Lett.* **111** 211803
[27] Himmel A and (Super-Kamiokande Collaboration) 2014 *AIP Conf. Proc.* **1604** 345
[28] Fogli G L, Lisi E, Marrone A, Montanino D, Palazzo A and Rotunno A M 2012 *Phys. Rev.* D **86** 013012
[29] Abe K *et al* (T2K Collaboration) 2015 *Phys. Rev.* D **91** 072010
[30] NAbgrall *et al* (NA61/SHINE Collaboration) 2011 *Phys. Rev.* C **84** 034604
[31] Abgrall N *et al* (NA61/SHINE Collaboration) 2012 *Phys. Rev.* C **85** 035210
[32] Abe K *et al* (T2K Collaboration) 2012 *Nucl. Instrum. Methods* A **694** 211
[33] Adamson P *et al* 2013 *Phys. Rev. Lett.* **110** 251801
[34] Adamson P *et al* 2011 *Phys. Rev. Lett* **106** 181801
[35] Hagiwara K, Mawatari K and Yokoya H 2004 *Phys. Lett.* B **591** 113
[36] Schreckenberger A 2013 *PhD Thesis* FERMILAB-THESIS-2013-4
[37] Adamson P *et al* 2010 *Phys. Rev.* D **81** 052004
[38] Adamson P *et al* 2011 *Phys. Rev. Lett.* **107** 011802
[39] Adamson P *et al* 2010 *Phys. Rev.* D **81** 072002
[40] Adamson P *et al* 2008 *Phys. Rev. Lett.* **101** 151601
Adamson P *et al* 2010 *Phys. Rev. Lett.* **105** 151601
Adamson P *et al* 2010 *Phys. Rev.* D **85** 031101R
Adamson P *et al* 2013 *Phys. Rev.* D **88** 072011
[41] Adamson P *et al* 2007 *Phys. Rev.* D **76** 052003
Osprey S *et al* 2009 *Geophys. Res. Lett.* **36** L05809
Adamson P *et al* 2010 *Phys. Rev.* **81** 012001
Adamson P *et al* 2011 *Astropart. Phys.* **34** 457
Adamson P *et al* 2011 *Phys. Rev.* D **83** 032011
Adamson P *et al* 2013 *Phys. Rev.* **87** 032005
[42] Abe K *et al* (T2K Collaboration) 2013 *Phys. Rev.* D **87** 092003
[43] Abe K *et al* (T2K Collaboration) 2014 *Phys. Rev. Lett.* **113** 241803

[44] Abe K *et al* (T2K Collaboration) 2014 *Phys. Rev.* D **90** 052010
[45] Abe K *et al* (T2K Collaboration) 2015 *Phys. Rev.* D **91** 112002
[46] Abe K *et al* (T2K Collaboration) 2014 *Phys. Rev.* D **90** 072012
[47] Abe K *et al* 2014 *Phys. Rev.* D **89** 092003
Abe K *et al* (T2K Collaboration) 2014 *Phys. Rev.* D **89** 099902 (addendum)
Abe K *et al* (T2K Collaboration) 2014 *Phys. Rev.* D **89** 099902 (erratum)
[48] Aguilar-Arevalo A A *et al* 2013 *Phys. Rev. Lett.* **110** 161801
[49] Sousa A and (MINOS, MINOS+ Collaborations) 2015 arXiv:hep-ex:1502.07715
[50] Hayato Y and (T2K Collaboration) 2009 *Acta Phys. Pol.* B **40** 2477
[51] Andreopoulos C *et al* 2010 *Nucl. Instrum. Methods* A **614** 87
[52] Abe K *et al* (T2K Collaboration) 2015 *Phys. Rev.* D **91** 051102
[53] Abe K *et al* (T2K Collaboration) 2015 *PTEP* **2015** 043C01
[54] Maki Z, Nakagawa M and Sakata S 1962 *Prog. Theor. Phys.* **28** 870
[55] Pontecorvo B 1968 *Sov. Phys.—JETP* **26** 984
Pontecorvo B 1967 *Zh. Eksp. Teor. Fiz.* **53** 1717
[56] Renshaw A *et al* (Super-Kamiokande Collaboration) 2014 *Phys. Rev. Lett.* **112** 091805
[57] Parke S J 2008 Neutrino oscillation phenomenology *Neutrino Oscillations* ed J A Thomas *et al* pp 1–18 FERMILAB-PUB-07-767-T
[58] Wolfenstein L 1978 *Phys. Rev.* D **17** 2369
Mikheyev S and Smirnov A 1985 *Sov. J. Nucl. Phys.* **42** 913